Published in final edited form as:

Neuron. 2019 August 21; 103(4): 686–701.e8. doi:10.1016/j.neuron.2019.05.038.

The Serotonergic Raphe Promote Sleep in Zebrafish and Mice

Grigorios Oikonomou[1,x], **Michael Altermatt**[1,x], **Rong wei Zhang**[1], **Gerard M. Coughlin**[1], **Christin Montz**[1], **Viviana Gradinaru**[1,*], **David A. Prober**[1,*,#]

[1]Division of Biology and Biological Engineering, California Institute of Technology, Pasadena, CA 91125, USA.

SUMMARY

The role of serotonin (5-HT) in sleep is controversial: early studies suggested a sleep-promoting role, but eventually the paradigm shifted towards a wake-promoting function for the serotonergic raphe. Here we provide evidence from zebrafish and mice that the raphe are critical for the initiation and maintenance of sleep. In zebrafish, genetic ablation of 5-HT production by the raphe reduces sleep, sleep depth and the homeostatic response to sleep deprivation. Pharmacological inhibition or ablation of the raphe reduces sleep, while optogenetic stimulation increases sleep. Similarly, in mice, ablation of the raphe increases wakefulness and impairs the homeostatic response to sleep deprivation, whereas tonic optogenetic stimulation at a rate similar to baseline activity induces sleep. Interestingly, burst optogenetic stimulation induces wakefulness in accordance with previously described burst activity of the raphe during arousing stimuli. These results indicate that the serotonergic system promotes sleep in both diurnal zebrafish and nocturnal rodents.

eTOC blurb

The wake-active serotonergic system (STS) has been considered part of the ascending arousal system that promotes wakefulness. Using zebrafish and mice, Oikonomou, Altermatt et al. demonstrate that the STS promotes sleep, potentially by generating homeostatic sleep pressure during wakefulness.

Keywords

Sleep; arousal; serotonin; 5-HT; raphe; optogenetics; fiber photometry

[*]Correspondence: viviana@caltech.edu (V.G.), dprober@caltech.edu (D.A.P.).

Author Contributions

G.O., M.A., D.P. and V.G. designed experiments. G.O. performed zebrafish experiments. M.A. performed mouse experiments. R.Z. performed zebrafish electrophysiology. G.M.C. performed mouse histology and quantification. C.M. isolated the zebrafish *tph2* promoter. V.G. supervised rodent aspects of the project. D.A.P. supervised zebrafish aspects of the project. G.O., M.A., V.G. and D.A.P. wrote the paper with input from R.Z. and G.M.C.

[X]These authors contributed equally

[#]Lead contact

Declaration of Interests

The authors declare no competing interests.

INTRODUCTION

The role of serotonin (5-HT) in sleep has been debated for over 50 years (Ursin, 2008). The multiple roles of the serotonergic system (STS) in animal physiology and behavior (Monti et al., 2008; Müller and Jacobs, 2010) make dissection of any specific aspect a challenge. In the central nervous system, the raphe, a diffuse network of brainstem nuclei, synthesize 5-HT and send projections to almost every region of the brain (Azmitia and Segal, 1978). Initial studies reported that ablation of the raphe in cats resulted in reduced 5-HT levels and sleep, in proportion to the size of the lesion (Jouvet, 1968). Intraperitoneal injections of *para*-chlorophenylalanine (pCPA), an irreversible inhibitor of tryptophan hydroxylase (TPH, the rate limiting enzyme in 5-HT synthesis), also reduced sleep (Koella et al., 1968; Mouret et al., 1968; Torda, 1967; Weitzman et al., 1968). This work, combined with studies of other neurotransmitters, gave rise to the monoaminergic theory of sleep (Jouvet, 1972), in which 5-HT plays an important sleep-promoting role. However, this paradigm eventually came into doubt (Monti, 2011; Ursin, 2008). Cooling of the dorsal raphe was shown to induce sleep in cats (Cespuglio et al., 1976), while in rats, raphe lesions were reported to cause hyperactivity with no effect on sleep (Bouhuys and Van Den Hoofdakker, 1977). The finding that most serotonergic raphe neurons are active during wakefulness, less active during non-rapid eye movement (NREM) sleep and mostly silent during rapid eye movement (REM) sleep (McGinty and Harper, 1976; Trulson and Jacobs, 1979), was taken as support for a wake-promoting role for 5-HT and the raphe. In addition, microdialysis studies showed that brain 5-HT levels follow a similar pattern with levels highest during waking, lower during NREM, and lowest during REM (Portas et al., 2000). Currently, the raphe are widely thought to promote wakefulness as part of the ascending arousal system (Saper et al., 2005; Scammell et al., 2017), although the debate is far from resolved (see Discussion).

We decided to investigate the role of 5-HT and the raphe in sleep using modern optogenetic and chemogenetic tools that enable neuronal manipulation with superior spatial and temporal precision. The conserved nature of both the STS and the sleep/wake cycle suggests that using a simple vertebrate system, which lacks the complex behavioral repertoire of murine systems that can confound interpretation of sleep studies, could provide insights translatable to mammals. The zebrafish is a well-established model system for the study of sleep (Oikonomou and Prober, 2017) with extensive anatomical and neurochemical homology to mammals, and has proven useful in uncovering conserved neuromodulatory circuits (Lovett-Barron et al., 2017). Here we show using both zebrafish and mice that the serotonergic raphe is a sleep-promoting system that is required for sleep homeostasis, but can also induce wakefulness in specific contexts. Our results support an evolutionarily conserved and mode-dependent role for the STS in regulating sleep.

RESULTS

Serotonin receptor agonists increase sleep and inhibition of 5-HT synthesis reduces sleep in zebrafish

We first sought to verify and expand upon previous pharmacological studies demonstrating a role for the STS in zebrafish sleep (Rihel et al., 2010). We treated zebrafish larvae with the

broad spectrum serotonergic receptor agonist quipazine, while monitoring their behavior using a videotracking system (Prober et al., 2006). Animals treated with quipazine showed a reduction in locomotor activity and increase in sleep compared to vehicle treated controls (Figures S1A-S1E). A reduction in waking activity (i.e. locomotor activity while awake) was also observed, indicating that activation of the STS induces an overall reduction in locomotion during wakefulness. Treatment with buspirone, a broad serotonergic receptor agonist with partial specificity for the inhibitory receptor 5-HT1A, gave similar results (Figures S1F-S1J). In both cases, night sleep phenotypes were associated with longer sleep bouts and reduced sleep latency (time to first sleep bout at night).

To broadly impair serotonergic signaling we used pCPA. Treated larvae had reduced 5-HT immunoreactivity (Figures S2A and S2B) (Airhart et al., 2012), as well as a significant increase in locomotor activity and decrease in sleep, due to fewer and shorter sleep bouts and a longer sleep latency (Figures S2C-S2G). These experiments suggest that the STS promotes sleep in zebrafish.

tph2−/− zebrafish do not produce 5-HT in the raphe and lack serotonergic brain innervation

In most vertebrates 5-HT is synthesized in several brain regions, including the pineal gland, preoptic area, posterior tuberculum, hypothalamus, midbrain/pons and medulla oblongata, with the raphe nuclei spanning the midbrain/pons boundary and medulla (Lillesaar, 2011). In placental mammals, brain 5-HT synthesis is limited to the pineal gland and the raphe nuclei. Hypothalamic (Vanhatalo and Soinila, 1998) and thalamic (Lebrand et al., 1996) neurons in mammals are 5-HT positive although they do not express TPH; instead they appear to take up 5-HT through the action of serotonin transporters (Vanhatalo and Soinila, 1998).

Staining for 5-HT in the larval zebrafish brain (Figure 1A) revealed several populations of 5-HT positive cells (Lillesaar et al., 2009; McLean and Fetcho, 2004). These include a small pretectal population, and large groups in the posterior tuberculum/hypothalamus which form a prominent horseshoe-like pattern. The pineal gland, where 5-HT serves as a substrate for the production of melatonin (Figure S3A), is also 5-HT positive (Figure 1A). In mammals, the raphe is subdivided into a rostral or superior group that lies on the midbrain/pons boundary (groups B5-B9, Dahlstroem and Fuxe, 1964) and includes the DRN and the median raphe nuclei (MRN), and a caudal or inferior group in the medulla (groups B1-B3). In zebrafish larvae, the raphe nuclei are also subdivided into superior raphe (SRa) and inferior raphe (IRa) (Figure 1A), while the dispersed medullary 5-HT-positive neurons have been excluded from the raphe designation, presumably because they do not express *tryptophan hydroxylase* (*tph*).

The zebrafish genome contains three *tph* paralogs (Bellipanni et al., 2002; Teraoka et al., 2004), of which only *tph2* is expressed in the raphe (Teraoka et al., 2004). We used genome editing to generate a zebrafish *tph2* predicted null mutant line (Chen et al., 2013). *tph2*−/− mice show severe developmental retardation and postnatal lethality (Alenina et al., 2009) which make interpretation of behavioral assays problematic. In contrast, *tph2*−/− zebrafish are healthy, develop normally and are born in Mendelian ratios, although some adults eventually develop scoliosis (data not shown). *tph2* mutant zebrafish lacked 5-HT immunoreactivity in the raphe and showed a dramatic reduction of 5-HT positive fibers

throughout the brain (Figure 1A). *tph2* is also expressed in the pretectal group and the pineal gland (Teraoka et al., 2004). In *tph2−/−* animals, 5-HT immunoreactivity was absent from the pretectal group, but the pineal gland still contained 5-HT, presumably due to expression of *tph1a* (Bellipanni et al., 2002), although the signal was reduced compared to sibling controls (Figure 1A). Interestingly, the medullary cells also lost 5-HT signal in *tph2−/−* animals even though these cells do not express *tph2*, suggesting that they take up extracellular 5-HT, similar to thalamic and hypothalamic populations in mammals. These observations corroborate previous studies demonstrating that the *tph2*-expressing raphe are the main source of serotonergic innervation in the zebrafish brain, similar to mammals (Lillesaar et al., 2009).

tph2−/− zebrafish show reduced sleep and altered sleep architecture

We next asked whether genetic loss of 5-HT affects sleep by in-crossing *tph2+/−* animals and monitoring their progeny. *tph2−/−* animals showed increased locomotor and waking activity and reduced sleep (Figures 1B-1F) compared to sibling controls. We observed no such differences between *tph2+/−* and *tph2+/+* animals. The mutant phenotype at night was due to shorter sleep bouts, with no effect on the number of sleep bouts (Figure 1F), suggesting that *tph2−/−* mutants enter sleep as often as controls but fail to maintain the sleep state for the normal amount of time. The mutants also showed an increase in sleep latency at night (Figure 1F). Thus, *tph2−/−* animals are defective in both initiating and maintaining the sleep state.

In the pineal gland, 5-HT is converted by arylalkylamine N-acetyltransferase 2 (AANAT2) to N-acetylserotonin, the substrate for the biosynthesis of melatonin (Figure S3A), a hormone that regulates sleep in mammals (Fisher et al., 2013) and zebrafish (Zhdanova et al., 2001; Gandhi et al., 2015). We hypothesized that the reduced sleep in *tph2* mutants could be caused not by reduced 5-HT in the raphe, but rather by reduced melatonin levels in the pineal gland due to reduced 5-HT. To test this hypothesis, we used *aanat2* mutant animals, which fail to synthesize melatonin and exhibit reduced sleep at night (Gandhi et al., 2015). We reasoned that if the *tph2* phenotype is caused solely by reduced melatonin levels, *aanat2* should be epistatic to *tph2,* that is, *aanat2*; *tph2* double mutants should show the same sleep phenotype as *aanat2* single mutants. Instead, we found that animals mutant for both *tph2* and *aanat2* slept less than either single mutant (Figures S3B-S3F), indicating that the sleep phenotypes of *tph2* and *aanat2* are additive and not epistatic to each other. This demonstrates that the *tph2−/−* phenotype is not due to reduced melatonin levels.

tph2−/− zebrafish show increased arousal, lighter sleep and attenuated sleep homeostasis

Since *tph2* mutants show reduced sleep, we asked whether they also exhibit a change in overall arousal. To assess this, we delivered mechano-acoustic stimuli of variable intensities at one-minute intervals during the night, while monitoring behavior (Singh et al., 2015). We determined the fraction of animals that responded to each stimulus, constructed stimulus-response curves (Figure 2A), and calculated the tapping power that resulted in half-maximal response (effective power 50, EP_{50}). The EP_{50} of *tph2−/−* animals was not significantly different from that of sibling controls, suggesting that although *tph2* mutants sleep less, they have a normal arousal threshold. However, the *tph2−/−* response curve had an elevated

plateau (Figure 2A), suggesting that *tph2* mutants exhibit increased arousal in response to strong stimuli.

To assay sleep depth, we applied the mechano-acoustic stimulus with an inter-trial interval of five minutes. This allows the animals to enter the sleep state between trials; thus, we were able to assay the response of awake or sleeping fish to a mild stimulus. We found that awake *tph2−/−* animals responded as efficiently as controls (Figure 2B left), but sleeping *tph2−/−* animals showed a significantly higher probability of responding to the stimulus (Figure 2B right). The observation that *tph2* mutants exit the sleep state more readily suggests a reduction in sleep depth.

The STS has been implicated in sleep homeostasis (see Discussion), so we asked whether zebrafish *tph2* mutants are defective in their response to sleep deprivation. To assay this, we crossed *tph2+/−* to *tph2−/−* animals and monitored the sleep profile of their progeny over a 48-hour period. On the beginning of the second night we subjected the animals to 6 hours of sleep deprivation (SD) by maintaining full daylight conditions, and then allowed them to enter recovery sleep by turning off the lights (Figure 2C). The Normalized SD Response (see STAR Methods) was significantly reduced in *tph2−/−* animals compared to sibling controls (Figure 2C). This reduced homeostatic response to sleep deprivation is in accordance with a previously-proposed role for the STS in sleep homeostasis (Jouvet, 1999). According to this hypothesis, STS activity and concomitant 5-HT release during the wake period are part of the build-up of homeostatic sleep pressure (see Discussion).

Zebrafish raphe neurons have higher firing rates during the day

Electrophysiological studies have shown that mammalian DRN serotonergic neurons have higher firing rates during wakefulness than during sleep (McGinty and Harper, 1976; Trulson and Jacobs, 1979). Serotonergic neurons have a “distinctive neuronal signature” that is used to identify them (Jacobs and Fornal, 2010), consisting of slow tonic firing (1-6 Hz) that is highly regular, and a long-duration action potential (2-3 ms). We asked whether larval zebrafish raphe 5-HT neurons show similar properties. We used a *Tg(tph2:eGFP)* line and fluorescence microscopy to identify such neurons and performed *in vivo* cell-attached recording to examine their spontaneous activity (Figure 2D). We found that they fire at 1-2 Hz (Figure 2E), with an action potential half-duration of 1-1.5 ms during the day (Figure 2F), similar to mammals. The firing rate was significantly reduced at night (Figure 2E), the main rest phase of zebrafish, similar to sleeping mammals. We also observed a reduction in the length of spontaneous action potentials during the night (Figure 2F). These observations demonstrate conserved electrophysiological properties between raphe 5-HT neurons of zebrafish and mammals.

Ablation of the raphe results in reduced sleep in zebrafish

Having established a sleep-promoting role for *tph2* in zebrafish, we asked whether cellular ablation of the raphe has a similar effect on behavior as genetic ablation of *tph2.* The *tph2* promoter is subject to positional effects (Yokogawa et al., 2012); thus using a 1.2 kb promoter fragment and screening multiple lines we generated a *Tg(tph2:eNTR-YFP)* line in which the *tph2* promoter drives expression of enhanced nitroreductase (Mathias et al., 2014;

Tabor et al., 2014) in the raphe, with no expression observed in the pineal gland or pretectal area (Figures 3A and 3A'). As previously described (Montgomery et al., 2016; Yokogawa et al., 2012), we observed sparse expression in the spinal cord for this and other *tph2* transgenic lines (data not shown). Unlike a previous transgene (Yokogawa et al., 2012), expression was not limited to the SRa, but instead included both the SRa and the IRa (Figure 3A). Nitroreductase converts the inert pro-drug metronidazole (MTZ) into a cytotoxic compound that causes cell-autonomous ablation (Curado et al., 2008). Following treatment with MTZ (Figures 3D-3F'), but not vehicle (Figures 3A-3C'), *Tg(tph2:eNTR-YFP)* animals lost both YFP and 5-HT immunoreactivity within the raphe soma and projections. Some 5-HT immunoreactive projections remained in the medulla, suggesting that these projections originate from medullary 5-HT positive cells and not the raphe (Figure 3E). After treatment with MTZ, *Tg(tph2:eNTR-YFP)* animals showed increased locomotor and waking activity, and reduced sleep, compared to sibling controls (Figures 3G-3K), similar to *tph2* mutants. These behavioral phenotypes were not simply due to the presence of the transgene, as vehicle-treated *Tg(tph2:eNTR-YFP)* animals behaved similarly to non-transgenic siblings (Figures S4A-S4E).

In order to verify that this phenotype is specific to loss of the raphe, we performed 2-photon laser ablation of the superior and inferior raphe at 4 dpf in *Tg(tph2:eGFP)* animals (Figure S4F) and assayed their behavior the next day. These animals showed increased locomotor activity and reduced sleep (Figure S4G-S4K), similar to the chemogenetic ablation phenotype. These results suggest that the raphe are necessary for normal sleep patterns, and have an overall sleep-promoting role in zebrafish.

Optogenetic stimulation of the raphe promotes sleep in zebrafish

Having shown that the raphe are necessary for normal amounts of sleep, we next asked whether their stimulation is sufficient to drive sleep. To address this question, we created a *Tg(tph2:ChR2-YFP)* transgenic line in which ChR2 (Lin et al., 2009) is expressed in the raphe (Figures 4A-4C). We used a modification of the videotracking system (Singh et al., 2015) to expose *Tg(tph2:ChR2-YFP)* animals and non-transgenic sibling controls to 30 minute pulses of blue light during the night, with a 90 minute inter-trial interval. These animals were maintained under dim light during the day in order to minimize background activation of ChR2; this still allows for normal wake/sleep cycles (Figures S5A-S5E). Upon exposure to blue light both populations of animals showed a brief spike in locomotor activity (presumably due to a startle response) followed by a return to baseline, and then a steady increase in activity during the period of illumination (Figure 4D). Transgenic animals showed reduced locomotor activity (Figure 4D) and increased sleep (Figure 4E) during illumination compared to sibling controls, suggesting that stimulation of the raphe promotes sleep. Interestingly, when we repeated this experiment using *tph2−/−* animals, stimulation of the raphe resulted in reduced locomotor activity (Figure 4F) but no increase in sleep (Figure 4G). A fraction of larval zebrafish raphe neurons produce GABA (Kawashima et al., 2016), which could mediate 5-HT-independent inhibition of locomotor activity. These results demonstrate that stimulation of the raphe is sufficient to both suppress locomotor activity and increase sleep, and that the sleep-promoting effect requires 5-HT.

The *Tg(tph2:ChR2-YFP)* line that we used showed YFP immunoreactivity in the pineal gland (Figures 4A'-4C') in addition to the raphe, although no expression was observed in the pretectal *tph2*-expressing population (Figures 4A-4C). Melatonin has high membrane permeability (Yu et al., 2016) and is thought to be released by passive diffusion (Simonneaux and Ribelayga, 2003), as opposed to being stored in vesicles which fuse with the cell membrane upon membrane depolarization. It is therefore unlikely that the sleep increase observed during exposure of *Tg(tph2:ChR2-YFP)* animals to blue light is due to an increase in melatonin release by the pineal gland. However, to experimentally address this possibility, we created *Tg(aanat2:ChR2-YFP)* animals, which express ChR2 exclusively in the pineal gland (Figures S5F-S5H'), and repeated the optogenetic experiment. We observed no difference in behavior between transgenic animals and non-transgenic sibling controls during blue light exposure (Figures S5I and S5J).

DRN neuronal activity correlates with sleep-wake states in mice

Encouraged by our zebrafish studies, we decided to revisit the question of sleep regulation by the STS in mammals. Previous studies used electrophysiology to record the activity of a few 5-HT neurons across sleep-wake states (McGinty and Harper, 1976) with cell-type determination based on electrophysiological characteristics, which do not allow for unequivocal identification of serotonergic neurons (Allers and Sharp, 2003; Kirby et al., 2003). To confirm these findings using genetically identified serotonergic neurons and investigate how the combined activity of large numbers of these neurons changes across sleep-wake states, we performed simultaneous polysomnographic (EEG/EMG) and fiber photometry (GCaMP) recordings in the DRN

SERT-cre mice (Zhuang et al., 2005), in which the serotonin transporter (SERT) promoter drives Cre expression specifically in 5-HT neurons, were implanted with EEG and EMG electrodes and injected with AAV5-Syn-Flex-GCaMP6s or AAV5-EF1a-DIO-eYFP, followed by optical fiber implantation targeting the DRN (Figures 5A, 5B and S6A). We quantified the specificity and efficiency of GCaMP6s+ neurons in the DRN of SERT-cre mice ($DRN^{SERT\text{-}GCaMP6s}$), and found that 93±1% of GCaMP6s-expressing neurons co-expressed TPH2, and that 81±3% of TPH2-expressing neurons co-expressed GCaMP6s. A representative example of an EEG spectrogram, behavioral state classification, EMG and $DRN^{SERT\text{-}GCaMP6s}$ signal is shown in Figure 5C. In agreement with electrophysiological studies, we observed the highest activity of DRN^{SERT} during wakefulness, followed by NREM and REM. Even though the baseline GCaMP6s signal decreased when animals transitioned from wake to NREM, we still observed bouts of increased DRN^{SERT} activity during periods classified as NREM. However, spectral analysis of EEG signals at a finer time scale suggests that these fluorescence peaks actually mark micro-awakenings (Figure S6B). Due to the short duration (<2 s; window size used for sleep/wake classification is 5 s) and small magnitude of changes in EMG, these periods were classified as NREM. $DRN^{SERT\text{-}eYFP}$ fiber photometry recordings displayed no such fluorescent variations (Figure S6C). To examine the dynamics of DRN^{SERT} population activity over the course of a particular state, fluorescent signals were extracted for each state, normalized with regard to time, and averaged across animals (Figure 5D). The summed neuronal activity level normalized by time was higher during wakefulness than in NREM and REM (Figure S6D).

Changes over time in $DRN^{SERT\text{-}GCaMP6s}$ fluorescence was observed for all states (Figure 5D), but only the decreases over the wake and NREM states were statistically significant (Figure S6E).

Next, we focused on changes in DRN^{SERT} activity at state transitions. Fluorescent signal of $DRN^{SERT\text{-}GCaMP6s}$ gradually decreased when an animal transitioned from wake to NREM (Figure 5E). Conversely, a time-locked increase in DRN^{SERT} activity occurred at the transition from NREM to wake (Figure 5F). When considering the activity during NREM >90 s before the transition to REM, DRN^{SERT} activity was lower during REM than in NREM (Figure 5G). Interestingly, $DRN^{SERT\text{-}GCaMP6s}$ fluorescence was lowest just before the transition from NREM to REM (Figure 5G), in agreement with single unit recordings (Trulson and Jacobs, 1979). When an animal transitioned from REM to wake, there was a time-locked increase in fluorescence (Figure 5H), similar to the NREM-to-wake transition. Taken together, these results verify and expand upon observations of putative 5-HT DRN neurons identified based on electrophysiological criteria, and provide insights into population activity across states and state transitions.

Ablation of serotonergic neurons leads to increased wakefulness and impairs the homeostatic response to sleep deprivation in mice

Early raphe physical ablation experiments resulted in reduced sleep (Jouvet, 1968), but this phenotype is complicated by the role of the medullary raphe in thermoregulation (Tan and Knight, 2018). Indeed, animals genetically engineered to lack all 5-HT neurons sleep less at an ambient temperature of 23°C but not at 33°C (Buchanan and Richerson, 2010), presumably due to shivering at 23°C, but not at the thermoneutral temperature of 33°C. We reasoned that targeted ablation of the superior raphe (groups B5-B9) while sparing the medullary populations (groups B1-B3) would avoid this complication. Therefore, we implanted SERT-cre mice with EEG and EMG electrodes and performed injections targeting the superior raphe with either AAV5-EF1a-mCherry-FLEX-dtA, which ablates cells expressing Cre recombinase, or a negative control virus (AAV5-EF1a-DIO-eYFP or AAV5-CAG-GFP) (Figures 6A and 6B). Two weeks later, sleep-wake patterns were recorded for 24 h. Subsequent histological analysis showed that only 5-HT neurons in the B5-B9 groups were ablated ($B5\text{-}B9^{SERT\text{-}dtA}$: 4±1%, n=8; $B5\text{-}B9^{SERT\text{-}eYFP}$ or $B5\text{-}B9^{GFP}$ 100±3%, n=9; unpaired t-test, $p<0.001$), whereas no change was observed in the B1-B3 groups ($B1\text{-}B3^{SERT\text{-}dtA}$: 104±6%, n = 8; $B1\text{-}B3^{SERT\text{-}eYFP}$ or $B1\text{-}B3^{GFP}$ 100±5%, n=9; unpaired t-test, $p>0.05$). The amount of wakefulness in experimental animals was increased at the expense of NREM and REM sleep during both the day and night (Figure 6C), in accordance with a sleep-promoting role for the superior raphe. $B5\text{-}B9^{SERT\text{-}dtA}$ animals had fewer wake bouts than controls (Figure 6E), but these wake bouts were longer than those of controls (Figure 6D, note log scale for Y-axis), resulting in increased time spent in wakefulness (Figure 6C).

To investigate the consequences of STS ablation on sleep homeostasis, animals were subjected to 6 h of SD at the beginning of the light phase following 24 h of baseline polysomnographic recordings. As expected, both $B5\text{-}B9^{SERT\text{-}dtA}$ and $B5\text{-}B9^{SERT\text{-}eYFP}$ or $B5\text{-}B9^{GFP}$ animals showed an increase in sleep following SD (recovery sleep), and the amount of time spent in wake, NREM or REM state during recovery was similar in both populations

(data not shown). A critical feature of recovery sleep is an increase in delta power during NREM (Borbely and Neuhaus, 1979). Indeed, both B5-B9$^{SERT\text{-}dtA}$ and B5-B9$^{SERT\text{-}eYFP}$ or B5-B9^{GFP} animals showed a significant increase in delta power during recovery sleep compared to baseline, although this effect was only significant for the first 2 h of recovery sleep for B5-B9$^{SERT\text{-}dtA}$ animals, whereas it remained significant for at least 6 h for B5-B9$^{SERT\text{-}eYFP}$ or B5-B9^{GFP} animals (Figures S7J and S7K). Furthermore, B5-B9$^{SERT\text{-}dtA}$ animals showed a significantly smaller increase in delta power compared to B5-B9$^{SERT\text{-}eYFP}$ or B5-B9^{GFP} (Figure 6F), suggesting that SD led to a smaller increase in homeostatic sleep pressure in B5-B9$^{SERT\text{-}dtA}$ animals. These results suggest that STS activity is normally involved in generating homeostatic sleep pressure, in accordance with the hypothesis put forward by Michel Jouvet (Jouvet, 1999; see Discussion).

Optogenetic stimulation of DRN neurons has bidirectional mode-dependent effects on mouse sleep

In addition to a tonic (~1-6 Hz) baseline firing pattern during wakefulness (McGinty and Harper, 1976), 5-HT neurons also fire in bursts (up to ~30 Hz) (Cohen et al., 2015; Liu et al., 2014; Schweimer and Ungless, 2010; Veasey et al., 1995). Therefore, we asked whether different stimulation modes can have different effects on sleep/wake states. To answer this question, we implanted SERT-cre mice with EEG and EMG electrodes, performed bilateral injections with either AAV5-EF1a-DIO-ChR2-eYFP or AAV5-EF1a-DIO-eYFP, and then implanted two optical fibers targeting the DRN (Figures 7A, 7B and S6A). We quantified the specificity and efficiency of ChR2+ neurons in the DRN of SERT-cre mice, and found that 94±1% of ChR2-expressing neurons co-expressed TPH2, and that 90±1% of TPH2-expressing neurons co-expressed ChR2. We then stimulated the raphe with either a burst or a tonic pattern (Figure 7C). Importantly, the number of stimuli per trial was the same for both stimulation modes. Based on results from preliminary experiments, burst stimulation experiments were conducted during the light phase, when mice are mostly asleep, and tonic stimulation experiments were conducted during the dark phase, when wake states dominate.

Burst optogenetic stimulation of DRN$^{SERT\text{-}ChR2}$ animals caused a sudden decrease in NREM and REM probability, and an increase in wake probability (Figure 7D). Changes in probability of sleep-wake states during the first minute of optogenetic stimulation were significantly different between DRN$^{SERT\text{-}ChR2}$ and DRN$^{SERT\text{-}eYFP}$ mice (Figure 7F). Tonic optogenetic stimulation of DRN$^{SERT\text{-}ChR2}$ caused an inhibition of REM similar to burst stimulation, however, it also caused an increase in NREM probability at the expense of wake probability over the course of stimulation (Figure 7G). Changes in probability of sleep-wake states during the last 5 minutes of optogenetic stimulation were different between DRN$^{SERT\text{-}ChR2}$ and DRN$^{SERT\text{-}eYFP}$ mice (Figure 7I). In DRN$^{SERT\text{-}eYFP}$ animals, neither burst nor tonic optogenetic stimulation affected behavioral states (Figures 7E, 7F, 7H and 7I). In order to determine whether optogenetic stimulation promotes initiation of a particular state, we investigated the latency to state transitions. We found that burst stimulation reduced the latency from NREM or REM to wake (Figure 7J), while tonic stimulation reduced the latency from wake to NREM (Figure 7J). We also asked whether optogenetic stimulation affects the duration of a particular state. Burst stimulation increased the duration of wake bouts (Figure S7A) and decreased the duration of NREM bouts (Figure S7B) while tonic

stimulation increased the duration of NREM bouts (Figure S7B) and decreased the duration of wake bouts (Figure S7A).

Spectral analysis demonstrated that burst stimulation of $DRN^{SERT\text{-}ChR2}$ animals reduced delta power, whereas tonic stimulation increased delta power, compared to $DRN^{SERT\text{-}eYFP}$ controls (Figure 7K). Conversely, burst stimulation increased, and tonic stimulation decreased, high frequency power (Figure 7L). These effects on patterns of brain activity are consistent with wake- and NREM-promoting effects of burst and tonic stimulation, respectively. Furthermore, as delta power is a measure of homeostatic sleep pressure (Borbély and Neuhaus, 1979), the increase observed under tonic stimulation is consistent with the idea that baseline STS activity (predominately 1-6 Hz) serves to build homeostatic sleep pressure (Jouvet, 1999).

To corroborate our results with an independent transgenic line, we performed similar experiments using the ePet-cre transgenic mouse line (Scott et al., 2005) (Figures S7E, S7F and S7H). Like the SERT-cre line (Zhuang et al., 2005), Cre recombinase is specifically expressed in CNS 5-HT neurons in ePet-cre mice. Surprisingly, neither burst nor tonic optogenetic stimulation of $DRN^{ePet\text{-}ChR2}$ animals had an effect on wake or sleep probability. The ePet-cre mouse line can show imperfect recombination efficiency (Narboux-Neme et al., 2013), so it is possible that fewer neurons were activated in this transgenic background. Indeed, histological quantification revealed that even though 96±1% ChR2-expressing neurons co-expressed TPH2, similar to the SERT-cre line (Figure S7C), only 28±2% TPH2-expressing neurons co-expressed ChR2 in ePet-cre mice, compared to 90±1% in SERT-cre mice (Figure S7D). This suggests that the lack of behavioral phenotypes during stimulation of $DRN^{ePet\text{-}ChR2}$ animals could be due to low levels of 5-HT release compared to SERT-cre mice. To test this hypothesis, we injected the selective serotonin reuptake inhibitor (SSRI) fluoxetine in $DRN^{ePet\text{-}ChR2}$ animals immediately prior to optogenetic stimulation to boost the optogenetically-induced increase in extracellular 5-HT concentration (Marcinkiewcz et al., 2016). In this context, burst and tonic stimulation resulted in increased wake and NREM probability (Figures S7G and S7I), respectively, similar to SERT-cre animals.

DISCUSSION

The debate regarding the role of the STS in sleep regulation has been carefully chronicled elsewhere (Ursin, 2008). In short, initial studies based on lesions and pharmacological inhibition of TPH supported a sleep-promoting role, but later the paradigm shifted in support of a wake-promoting role, mostly due to the wake-active nature of 5-HT DRN neurons. The debate has continued in the modern era with pharmacological work generating conflicting results. For example, ritanserin, an antagonist of the excitatory 5-HT2 receptor family, promotes sleep in humans (Idzikowski et al., 1986) and rats (Dugovic and Wauquier, 1987), but wakefulness in cats (Sommerfelt and Ursin, 1993), while agonists of the inhibitory 5-HT1A receptor decrease wakefulness when administered locally, but increase wakefulness when administered systemically (Portas and Grønli, 2008). Genetic models have often contradicted pharmacology (Adrien, 2008): mice mutant for 5-HT2A show reduced sleep, but treatment with a 5-HT2A receptor antagonist increases sleep (Popa, 2005). However, genetic studies can also be difficult to interpret: while embryonic ablation of *tph2* was

reported to not alter total sleep levels in mice (Solarewicz et al., 2015), these results are complicated by severe developmental retardation and postnatal lethality in these animals (Alenina et al., 2009). Genetic ablation of *tph2* in the pons/midbrain raphe nuclei (groups B5-B9) of adult mice was shown to cause hyperactivity and eliminate siestas (Whitney et al., 2016), although ablation of the majority of serotonergic neurons in both the midbrain/pons and medulla of adults using an ePet-cre line caused a reduction only in REM sleep (Iwasaki et al., 2018). Optogenetic inhibition of 5-HT DRN neurons using ePet-cre blocked arousal in response to high levels of CO_2 (Smith et al., 2018), suggesting that the DRN is required for wakefulness induced by hypercapnia.

To limit confounds generated by the diverse role of the STS in animal behavior (Müller and Jacobs, 2010), we first investigated sleep-regulating aspects of the STS in the larval zebrafish, a diurnal vertebrate which displays robust sleep cycles (Prober et al., 2006) but lacks a complicated behavioral repertoire (Dreosti et al., 2015). Our larval zebrafish work supports a sleep-promoting role for the STS. Serotonin receptor agonists increase sleep and TPH inhibition reduces sleep. *tph2* mutant animals exhibit reduced and lighter sleep, increased maximal arousal, and reduced homeostatic response to sleep deprivation. Ablation of the raphe phenocopies the *tph2* mutant phenotype, while optogenetic stimulation increases sleep in a *tph2*-dependent fashion. Interestingly, the electrophysiological properties of the 5-HT raphe neurons of larval zebrafish are similar to those of mammals: they fire at a regular and slow rate which is elevated during the wake period, and their action potentials are long-lasting.

In mammals, early studies describing the firing pattern of 5-HT neurons were based on single-unit recordings and used electrophysiological criteria to differentiate between serotonergic neurons and other DRN cell types. However, these criteria do not allow for unequivocal identification of serotonergic neurons as non-serotonergic DRN neurons can have similar firing properties (Allers and Sharp, 2003; Kirby et al., 2003). We therefore used fiber photometry to record the activity of genetically identified 5-HT neurons. Our findings confirm results from single-unit recordings (McGinty and Harper, 1976; Trulson and Jacobs, 1979), wherein serotonergic DRN neurons display the highest activity level during the wake state, followed by NREM and REM. Early studies in which 5-HT production was pharmacologically inhibited or the DRN were physically ablated showed a reduction in sleep (Jouvet, 1968; Mouret et al., 1968), but this phenotype was later attributed to increased shivering due to disrupted thermoregulation (Buchanan and Richerson, 2010; Murray et al., 2015). To avoid this complication, we selectively targeted the superior raphe, while leaving intact the thermoregulatory populations in the medulla, and observed a reduction in sleep. Optogenetic activation of the DRN in a tonic pattern, at a frequency similar to that of endogenous baseline activity, reduced wake and REM probability with a concurrent increase in NREM probability. Thus, in both zebrafish and mice the STS appears to play a sleep-promoting role.

Our work in zebrafish and mice, as well as classical studies in mammals (McGinty and Harper, 1976; Trulson and Jacobs, 1979) generate an apparent paradox: how can a sleep-promoting system be more active during wakefulness? Michel Jouvet sought to reconcile this paradox by proposing a role for the STS in sleep homeostasis (Jouvet, 1999). According

to the two-process model (Borbély, 1982), sleep is regulated by a circadian component (process C), which gates the timing of sleep, and a homeostatic component (process S), which builds sleep pressure during wakefulness. The sleep pressure generated by process S is eventually relieved when the animal enters the sleep state at the time prescribed by process C. Jouvet proposed that the activity of the STS and concomitant release of 5-HT during wakefulness are part of process S and serve to build sleep pressure by measuring the duration and intensity of waking (Jouvet, 1999), presumably along with other somnogenic molecules such as adenosine (Porkka-Heiskanen et al., 1997). Indeed in *Drosophila,* 5-HT promotes sleep and *5HT1* mutants show reduced sleep, as well as reduced rebound sleep following sleep deprivation, in accordance with a role for 5-HT in measuring sleep debt (Yuan et al., 2006). Flies mutant for *trh* (equivalent to *tph*) or the serotonin receptor *5HT2b* have reduced homeostatic response to sleep deprivation, and a small group of *5HT2b*-expressing neurons in the dorsal fan-shaped body is necessary for rebound sleep (Qian et al., 2017). Mice mutant for *5-HT2A* sleep less and, following sleep deprivation, show a smaller delta power increase compared to controls (Popa, 2005), suggesting a reduced homeostatic sleep drive. Mice mutant for *5-HT2C* also show reduced sleep and disrupted sleep homeostasis (Frank et al., 2002). Here we show that *tph2* mutant zebrafish have reduced response to sleep deprivation, that raphe-ablated mice show reduced increase in delta power after sleep deprivation, and that tonic optogenetic activation of the raphe in mice increases delta power. These results support Jouvet's hypothesis that the STS promotes sleep, despite being wake-active, by forming part of the sleep homeostasis system. Thus, the induction of sleep during optogenetic activation of the STS in zebrafish and mice, described here, could be due to a transient increase in sleep pressure.

Distinct and even opposing effects during tonic versus burst activity have been reported for other monoaminergic systems, including dopamine (Goto et al., 2007) and noradrenaline (Aston-Jones and Cohen, 2005). Recently, tonic activation of centromedial thalamic neurons in mice was shown to induce wakefulness, while burst activation induced slow-wave-like activity and enhanced cortical synchrony (Gent et al., 2018). These studies suggest that different activity modes of the same circuit can have opposite behavioral outcomes. Indeed, contrary to tonic stimulation, burst stimulation of the DRN in mice increased wake probability at the expense of NREM and REM. Whereas tonic activity is the typical mode observed in the raphe (Jacobs and Azmitia, 1992), burst activity occurs in specific contexts including reward/punishment (Cohen et al., 2015; Liu et al., 2014), treadmill-induced locomotion (Veasey et al., 1995) and noxious stimuli (Schweimer and Ungless, 2010), all of which are presumably arousing. Thus, we propose that the endogenous baseline mode of tonic activity mediates the sleep-promoting role of the STS, while burst activity is a component of arousal-inducing behaviors. The correlation between burst activity and noxious stimuli suggests that hypercapnia-induced arousal might involve burst firing of STS neurons. The mechanisms that enable different modes of activity by the STS to generate opposing behavioral outcomes are unclear. In the leech Retzius neuron, tonic stimulation at 1 Hz generates only synaptic release of 5-HT, but burst stimulation at 10 or 20 Hz generates extrasynaptic release of 5-HT from the soma and axonal varicosities (Trueta and De-Miguel, 2012). Thus, different modes of STS activity could translate into different spatial or quantitative patterns of 5-HT release. Alternatively, tonic and burst modes of activity could

recruit different serotonergic sub-systems. It has recently been shown that the DRN consists of anatomic subdivisions with distinct inputs, outputs and functionalities (Ren et al., 2018). It is possible that these sub-systems employ inherently different modes of activity and hence are preferentially recruited by burst versus tonic inputs. Considering that these two hypotheses are not mutually exclusive, and that the number of sub-systems that comprise the STS is likely to increase along with our understanding of it, a significant effort will be required in order to fully elucidate the bimodal effects of the STS on sleep/wake states and on other behaviors.

STAR METHODS

CONTACT FOR REAGENT AND RESOURCE SHARING

Further information and requests for resources and reagents from zebrafish or mouse experiments should be directed to and will be fulfilled by David Prober (dprober@caltech.edu).

EXPERIMENTAL MODEL AND SUBJECT DETAILS

Animal husbandry and all experimental procedures involving animals were performed in accordance with the California Institute of Technology Institutional Animal Care and Use Committee (IACUC) guidelines and by the Office of Laboratory Animal Resources at the California Institute of Technology (animal protocols 1580 (zebrafish) and 1672 (mice)).

Zebrafish—All experiments used healthy zebrafish between 4 and 7 dpf; at this stage of development, sex is not yet defined. Larvae were housed in petri dishes with 50 animals per dish. E3 medium (5 mM NaCl, 0.17 mM KCl, 0.33 mM $CaCl_2$, 0.33 mM $MgSO_4$) was used for housing and experiments. All lines were derived from the TLAB hybrid strain. Animals were not involved in any previous procedures and were naive to the tests and drugs used.

Mice—SERT-cre (Zhuang et al., 2005) and ePet-cre (Scott et al., 2005) mice were crossed to wild type C57BL/6 mice (Charles River). All animals had a normal immune status. Only male animals heterozygous for the Cre transgene were used for experiments. After weaning, animals of the same gender were group-housed until they underwent surgery at the age of 6-12 weeks. After surgery, subjects were single-housed for at least five days in a residence room for full recovery before animals were moved to a behavioral room. In the behavioral room, animals were housed on a 12:12 h light/dark cycle (light off at 6 a.m. and light on at 6 p.m.) with ad libitum access to food and water. Mice were acclimated to the new behavioral room and light/dark cycle for at least 2 weeks before experiments were started. Animals used for experiments were not involved in any previous procedures and were naive to the tests and drugs used.

METHOD DETAILS

Zebrafish Methods and Data Analysis

Pharmacology (zebrafish): Quipazine maleate salt (Q1004, MilliporeSigma, Burlington, MA, USA), buspirone hydrochloride (B7148, MilliporeSigma, Burlington, MA, USA) and 4-Chloro-DL-phenylalanine methyl ester hydrochloride (pCPA) (C3635, MilliporeSigma,

Burlington, MA, USA) were dissolved in dimethyl sulfoxide (DMSO) and added to E3 medium (5 mM NaCl, 0.17 mM KCl, 0.33 mM $CaCl_2$, 0.33 mM $MgSO_4$, pH 7.4) for a final concentration of 0.1% DMSO and 10 μM quipazine, 25 μM buspirone or 7.5 μM pCPA. These concentrations were determined through dose-response experiments (0.1 μM to 100 μM), and allow for robust behavioral phenotypes without apparent toxicity or abnormal responses to a gentle stimulus. Controls were exposed to 0.1% DMSO alone. For sleep/wake experiments, drugs were added during the evening of the 4th day of development; reported data is from the 5th day and night of development.

Transgenic and mutant animals (zebrafish): For the construction of *Tg(tph2:ChR2-YFP)* and *Tg(tph2:eNTR-YFP)* lines, a 1.2 kb genomic fragment from the promoter region of *tph2* was amplified using primers 5'-TGTCTTCCTGCCATTAGTCTG-3' (forward) and 5'-TTAATATGGCAAAGGTAGTTTTTTTTATC-3' (reverse) into a vector containing NRSE elements and Tol2 recognition sequences. This promoter fragment is subject to positional effects; depending on the integration site in the genome it can drive expression in all or subsets of the reported CNS *tph2* expression sites (pineal gland, pretectal area, raphe). *Tg(tph2:ChR2-YFP)* animals showed YFP immunoreactivity in the pineal gland and the raphe, while *Tg(tph2:eNTR-YFP)* animals only showed expression in the raphe. Both lines also show sparse expression in the spinal cord, as previously shown for other *tph2* transgenic lines (Yokogawa et al., 2012). For the construction of *tph2* mutants, TALEN-based genomic editing was used to introduce a 4 bp insertion in exon 6 of *tph2* (ENSDARG00000057239) (Chen et al., 2013), which causes a frameshift at nucleotide 721 (out of 1427) of the open reading frame and introduces multiple premature stop codons (first stop codon appears at nucleotide 841). For genotyping, genomic DNA was prepared using standard methods (Westerfield, 2000) and PCR was performed using a set of 3 primers (5'-AGAACTTACAAAACTCTATCCAACTC-3', 5'-AGAGAGGACAACATCTGGGG-3', 5'-TAATCATGCAGTCCGTTAATACTC-3'), which produce one band for homozygous wild-type animals (255 bp), two bands for homozygous mutant animals (177 bp and 259 bp), and three bands for heterozygous mutant animals (177 bp, 255 bp and 259 bp). PCR products were run on a 4% agarose gel.

Immunohistochemistry (zebrafish): Samples were fixed in 4% PFA/4% sucrose in PBS overnight at 4°C and then washed with 0.25% Triton X-100/PBS (PBTx). Immunolabeling was generally performed using dissected brains because dissection allows for superior antibody penetration. However, for pineal gland imaging whole-mount staining was performed because the pineal gland is often damaged by dissection. Whole larvae or dissected brains were incubated for 1 h in 1 mg/mL collagenase (C9891, MilliporeSigma, St. Louis, Missouri, USA) and blocked overnight in 2% NGS/2% DMSO in PBTx at 4°C. Antibody incubations were performed in blocking solution overnight at 4°C. Primary antibodies were rabbit anti-5-HT (1:1000; S5545, MilliporeSigma, Burlington, MA, USA) and chicken anti-GFP (1:400; GFP-1020, Aves Labs, Tigard, OR, USA). Secondary antibodies were goat anti-Chicken IgY (H+L), Alexa Fluor 488 (1:500; A-11039; Invitrogen, Carlsbad, CA, USA) and goat anti-Rabbit IgG (H+L) cross-adsorbed, Alexa Fluor 568 (1:500; A-11011; Invitrogen, Carlsbad, CA, USA). Samples were mounted in Vectashield

(H-1000; Vector Laboratories, Burlingame, CA) and imaged using a Zeiss LSM 780 or Zeiss LSM 880 confocal microscope (Zeiss, Oberkochen, Germany).

Electrophysiological recordings (zebrafish): For cell-attached recordings of raphe neurons, we used 4- to 6-dpf *Tg(tph2:eGFP)* animals, in which serotonergic raphe neurons were visualized using a fluorescent microscope (BX50WI, Olympus, Tokyo, Japan) and an infrared CCD camera (IR1000, DAGE-MTI, Michigan City, IN, USA). Animals were paralyzed by bath application of 0.1% α-bungarotoxin (2133, Tocris Bioscience, Bristol, UK) for 10-15 min, then embedded in a custom-made glass-bottom petri dish with 1.5% low-melting agarose (A9414, MilliporeSigma, Burlington, MA, USA) dorsal side up, and immersed in extracellular solution (134 mM NaCl, 2.9 mM KCl, 2.1 mM $CaCl_2$, 1.2 mM $MgCl_2$, 10 mM HEPES, 10 mM glucose; 290 mOsmol/L, pH = 7.8). A small incision was made at the skin above the ventricle between cerebellum and hindbrain using a glass micropipette. Micropipettes were made from borosilicate glass (BF100-58-10, Sutter Instrument, Novato, CA, USA) by a Flaming/Brown micropipette puller P-87 (Sutter Instrument, Novato, CA, USA). The recording pipette (~10 MΩ in resistance, ~2 μm tip opening) was filled with extracellular solution, and advanced into the brain through a motorized micromanipulator (MP-225, Sutter Instruments, CA, USA). Contact of the micropipette onto raphe neurons was confirmed by visualizing eGFP-positive membranes within the tip of the recording micropipette. Spike firing was detected by a MultiClamp 700B amplifier (Molecular Devices, San Jose, CA, USA) and a 1550B4 Digidata data acquisition system (Molecular devices, CA, USA). Signals were filtered at 2 kHz and sampled at 10 kHz. To avoid baseline fluctuations, signals were recorded with a 1 Hz high pass filter.

Chemogenetic ablation (zebrafish): Animals were treated with 5 mM metronidazole (MTZ) (0215571080, MP Biomedicals, Santa Ana, CA, USA) diluted in E3 medium containing 0.2% DMSO, starting in the afternoon at 2 dpf, and refreshed every 24 h. Animals were kept in dim light during the day to prevent MTZ photodegradation. In the evening at 4 dpf, the animals were rinsed 3 times in E3 medium and then transferred to behavioral plates. Reported data is from the 5th day and night of development.

2-Photon laser ablation (zebrafish): 4 dpf *Tg(tph2:eGFP); nacre* animals were anesthetized in E3 medium containing 0.016% tricaine (A5040, MilliporeSigma, Burlington, MA, USA) and mounted in 1.5% low-melting agarose (A9414, MilliporeSigma, Burlington, MA, USA) dorsal side up. 2-Photon laser ablation of the raphe was performed using a Zeiss LSM 880 microscope (Zeiss, Oberkochen, Germany) equipped with a Titanium:Sapphire two-photon laser (Chameleon Ultra II, Coherent, Santa Clara, CA) and 20x water immersion objective (1.0 NA). To create local lesions the bleaching function of the Zen Black software (Zeiss, Oberkochen, Germany) was used with the following parameters: pixel dwell time 2.06 μsec, pixel size 0.42 μm, laser power 100% (~3700 mW), 30 iterations. All GFP positive cells around a 200 μm caudal-to-rostral axis along the midline starting from the caudal tip of the superior raphe were ablated (approximately 100 cells/animal). This area includes all of the superior raphe and the majority of the inferior raphe. Cells were ablated one at a time, or in case of closely arranged cells, in groups no larger than 3-4 cells.

Ablations were considered successful when no GFP was observable and a small cavitation was briefly visible after treatment. Mock ablated controls were mounted next to the ablated animals. After ablation/mock ablation, animals were unmounted, transferred to the videotracking system and allowed to recover overnight before assaying behavior at 5 dpf.

Optogenetics (zebrafish): The videotracking system was modified to include a custom array containing three sets of blue LEDs (470 nm, MR-B0040-10S, Luxeon V-star, Brantford, Canada) mounted 15 cm above and 7 cm away from the center of the 96-well plate to ensure uniform illumination. The LEDs were controlled using a custom-built driver and software written in BASIC stamp editor. A power meter (1098293, Laser-check, Santa Clara, CA, United States) was used before each experiment to verify uniform light intensity (~500 μW at the surface of the 96-well plate). In the morning of the fifth day of development, single larvae were placed into each well of a 96-well plate and placed in the videotracker. Larvae were exposed to blue light for 30 min with at least 60 min of recovery between trials. Total locomotor activity for each larva was monitored for 30 min before and after light onset. Light onset induces a startle response, which causes a short burst of locomotor activity. For this reason, we excluded 5 min of behavioral recording centering around the peak of the startle response from analysis. The two minutes before light offset was also excluded from analysis. For normalization, the locomotor activity and sleep of each larva during light exposure was divided by the average baseline locomotor activity and sleep for all larvae of the same genotype. For baseline, we used a time period equal to blue light treatment, but prior to light onset.

Sleep/wake analysis (zebrafish): Sleep/wake analysis was performed as previously described (Prober et al., 2006). Larvae were raised on a 14:10 h light:dark (LD) cycle at 28.5°C with lights on at 9 a.m. and off at 11 p.m. Dim white light was used to raise larvae for optogenetic experiments to prevent stimulation of ChR2 by ambient light. Individual larvae were placed into each well of a 96-well plate (7701-1651, Whatman, Pittsburgh, PA, United States) containing 650 μl of E3 embryo medium. Locomotor activity was monitored using a videotracking system (Viewpoint Life Sciences, Lyon, France) with a Dinion one-third inch Monochrome camera (Dragonfly 2, Point Grey, Richmond, Canada) fitted with a variable-focus megapixel lens (M5018-MP, Computar, Cary, NC, United States) and infrared filter. The movement of each larva was recorded using the quantization mode. The 96-well plate and camera were housed inside a custom-modified Zebrabox (Viewpoint Life Sciences) that was continuously illuminated with infrared lights. The 96-well plate was housed in a chamber filled with recirculating water to maintain a constant temperature of 28.5°C. The parameters used for movement detection were: detection threshold, 15; burst, 29; freeze, 3; bin size, 60 s, which were determined empirically. Data were analyzed using custom Perl and Matlab (Mathworks, Natick, MA, United States) scripts (Source code 1), which conform to the open source definition. For this and all behavioral assays, animals were genotyped after the experiment to identify mutant, transgenic and control animals.

Sleep deprivation (zebrafish): Sleep deprivation (SD) was performed on 6 dpf animals during the first 6 h of the subjective night by maintaining daytime levels of illumination. Animals that failed to show at least a 50% reduction in sleep during the first 4 h of sleep

deprivation (SD Sleep) compared to sleep during the first 4 h of the previous night (Baseline Sleep) were excluded from analysis. For each genotype we defined Sleep Lost as the difference between Baseline Sleep and SD sleep averaged for all animals of that genotype. Normalized SD Response was defined as the ratio of Recovery Sleep (i.e. sleep during the first 4 h after sleep deprivation) for each animal to Sleep Lost. Only 4 h of Recovery Sleep (and hence Baseline Sleep) were used in order to ensure that all sleep data were confined to the circadian night (6 h of SD + 4 h of Recovery Sleep for a total of 10 h of circadian night per standard zebrafish rearing protocols).

Arousal analysis (zebrafish): The videotracking system was modified by adding an Arduino (http://www.arduino.cc/) based automated driver to control two solenoids (28P-I-12, Guardian Electric, Woodstock, IL, United States) that delivered a tap to a 96-well plate containing zebrafish larvae (Gandhi et al., 2015). This setup allowed us to drive the solenoids with voltage ranging from 0 V to 20 V over a range of 4095 settings (from 0.01 to 40.95). In our experiments, we used taps ranging from a power setting of 1–36.31. Taps of 14 different intensities were applied in a pseudo-random order from 12:30 a.m. to 7:30 a.m. during the fifth night of development with an inter-trial-interval (ITI) of 1 min. Previous studies showed that a 15 s interval between repetitive stimuli is sufficient to prevent behavioral habituation (Burgess and Granato, 2007). The background probability of movement was calculated by identifying for each genotype the fraction of larvae that moved 5 s prior to all stimuli delivered during an experiment (14 different tap powers × 30 trials per experiment = 420 data points per larva; average background movement). This value was subtracted from the average response fraction value for each tap event (corrected response = average response – average background movement). For sleep depth analysis, taps were delivered every 5 min at powers low enough to allow discrimination between awake and sleeping fish. The response of larvae to the stimuli was monitored using the videotracking software and was analyzed using Matlab (Mathworks) and Excel (Microsoft, Redmond, WA, United States). Statistical analysis was performed using the Variable Slope log(dose) response curve fitting module of Prism (Graphpad, La Jolla, CA, United States) for 1 min ITI and the Kruskal-Wallis test for 5 min ITI.

Mouse Methods and Data Analysis

Surgical Procedures (mouse)

General: Adult mice were anesthetized with isoflurane (5% induction, 1% maintenance). After weighing the animal, ketoprofen (5 mg/kg) and buprenorphine SR (1 mg/kg) were subcutaneously injected. The mouse was placed on a stereotaxic frame (David Kopf Instruments, CA, USA) and body temperature was kept stable throughout the surgery with a heating pad. The hair covering the skin above the skull was removed and the skin was sterilized with chlorhexidine. A sterile scalpel was used to make an incision. The skull was cleaned with autoclaved cotton swabs. Bregma and lambda were leveled to be on the same z-axis. Two points on the surface of the skull 2.5 mm to either side of lambda were used to level the skull with regard to the y-axis. After further surgical procedures detailed below, Bupivacaine (up to 1 mg/kg) is applied subcutaneously to the skin margins at the site of the incision to provide local analgesia before closing the wound. Tissue adhesive was used to

close the incision. During the post-operative care period, mice were provided with ibuprofen (30 mg/kg) in the drinking water.

Viral injection: To inject virus and implant optical fibers for optogenetic and fiber photometry experiments, craniotomy holes were made over the dorsal raphe nucleus (DRN; antero-posterior (AP) axis: −4.65 mm; medio-lateral (ML) axis: ±1.3 mm; relative to Bregma). Virus was injected using a blunt 33 or 35-gauge microinjection needle within a 10 uL microsyringe (NanoFil, World Precision Instruments, FL, USA). The injection needle was lowered at an angle into the DRN (AP: −4.65 mm; ML: ±1.30 mm; dorsoventral (DV): −2.9~3.05 mm, at a 20 degree angle relative to vertical axis). Injection volume was controlled by a microsyringe pump (UMP3, World Precision Instruments), which was connected to a controller (Micro4, World Precision Instruments). 0.5-1 μL of AAV was infused per site at a rate of 100 nL per min. After injection, the needle was kept in place for an additional 10 min to allow the virus to diffuse into the tissue. To avoid backflow, the needle was withdrawn over approximately 10 min. Following each injection, the needle was rinsed multiple times with sterile saline to prevent clogging in subsequent injections. For fiber photometry experiments, mice were unilaterally injected with 1 μL AAV5-Syn-FLEX-GCaMP6s (1×10^{13} genome copies/mL) or AAV5-Ef1a-DIO-eYFP (1×10^{13} genome copies/mL). For optogenetic experiments, mice were bilaterally injected with 0.5 μL AAV5-Ef1a-DIO-ChR2(H134R)-eYFP ($1\text{-}2.5\times10^{13}$ genome copies/mL) or AAV5-Ef1a-DIO-eYFP (1×10^{13} genome copies/mL).

The procedure was the same for ablation experiments, but the number of craniotomies, injection coordinates and volumes were different (AP: −4.1, −4.4, −4.4, −4.6 mm; ML: −1.65, −1.3, +1.6, +1.3 mm; dorsoventral (DV): −4.85, −3.1, −4.8, −3.1 mm, at a 20 degree angle relative to vertical axis; injection volumes from anterior to posterior: 0.5, 1, 0.5, 0.5 μL).

For ablation experiments we targeted all non-medullary 5-HT populations (groups B5-B9) as opposed to only the DRN (groups B6-B7) which were the target of our fiber photometry and optogenetics experiments. We made this choice for three reasons: First, in our chemogenetic and 2-photon ablations in zebrafish we ablated all non-medullary populations. Therefore, ablating groups B5-B9 in mice would allow for direct comparison between the two species. Second, previous work has suggested that other non-medullary raphe nuclei beyond the DRN are involved in sleep regulation (Jouvet, 1968). Third, ablating specifically groups B6-B7 (DRN) is technically challenging as they are anatomically very close to the smaller groups B5, B8 and B9. Indeed, interpretation of past ablation-based work has at times been complicated by questions of specificity. In optogenetic and fiber photometry experiments possible transfection of non-DRN populations is not an issue, since the localization of the optical fiber and the limited ability of light to travel through tissue allow for precise targeting (and also only allow a small area to be targeted). In the case of AAV5-EF1a-mCherry-FLEX-dtA injections, diffusion of AAVs through the tissue does not allow for precise targeting; efforts to limit dtA expression to only groups B6-B7 would result in a cohort of mice with varying levels of ablation coverage. Therefore, to ensure consistency, we decided to target all non-medullary groups instead, in agreement with a previous raphe-ablation study (Whitney et al., 2016). Importantly, this strategy spares the B1-B3 groups

(Figure 6B), ablation of which has been shown to secondarily disrupt sleep due to the role of these groups in thermoregulation.

Whenever possible, cage mates were split into experimental and control groups. Allocation of animals to experimental and control groups was random. Behavioral experiments were started no earlier than 14 days after injection to ensure sufficient viral transgene expression.

Optical fiber implantation: After the injection needle was withdrawn, optical fibers with cut length of 4 mm (optogenetics: MFC_300/330-0.37_4mm_ZF1.25_FLT, fiber photometry: MFC_400/430-0.48_4mm_ZF1.25_FLT, Doric lenses, Quebec, QC, Canada) were mounted in a stereotaxic holder (1766AP, David Kopf Instruments, CA, USA) and inserted into the tissue targeting the DRN (AP: −4.65 mm; ML: ±1.30 mm; DV: −2.5~2.75 mm, at a 20 degree angle relative to vertical axis, see Figures S6A and S7E). For fiber photometry experiments only one optical fiber was implanted per animal, whereas two optical fibers were bilaterally inserted for optogenetic experiments. To fix the optical fibers to the skull, a layer of adhesive cement (C&B Metabond, Parkell Inc., NY, USA) was applied to the surface of the skull around the optical fiber. In addition, a layer of dental cement (51458, Stoelting Co., IL, USA) was used to secure the optical fiber.

EEG and EMG implantation: For EEG/EMG recordings, three craniotomy holes were made (for reference and ground: AP: −3.2 mm; ML: −2.8 mm; for first EEG channel: AP: 1.7 mm; ML: 0.8 mm; for second EEG channel: AP: −1.3 mm; ML: 1.3 mm) with a drill bit (#73, 105-0240.340, Kyocera, Kyoto, Japan). 0.10” electrodes with wire lead (8403, Pinnacle Technology Inc., KS, USA) were screwed into the craniotomy holes. Electrodes were covered and fixed to the skull with adhesive cement. Lead wires from the screw electrodes were connected to an EEG/EMG headmount (8201, Pinnacle Technology Inc.). Connections between lead wires and headmount were covered with silver epoxy (MG Chemicals, BC, Canada) to ensure electrical conduction. EMG wires from the headmount were inserted into the trapezius muscles. Dental cement was used to cover wires and their connection to the headmount.

Histology (mouse)

Perfusion: Animals were euthanized with 100 mg/kg euthasol i.p. injection and transcardially perfused with ice-cold 1x phosphate buffered saline (PBS) followed by ice-cold 4% paraformaldehyde (PFA) in 1x PBS. Mouse brains were post-fixed in 4% PFA at 4Ό overnight on a sha ker. Samples were immersed in 30% sucrose in 1x PBS solution for >2 days. Mouse brains were then embedded in Tissue-Tek O.C.T. Compound (102094-104, VWR) before freezing in dry ice for 1 h. Samples were then transferred to a −80°C freezer for long-term sto rage or directly sliced on a cryostat (Leica Biosystems). Samples from optogenetic and fiber photometry experiments were sectioned into 30 μm slices covering the superior (pontine) raphe. Samples from ablation experiments covered both the superior and inferior (medullary) raphe and were hence sectioned into 50 μm slices to reduce the number of sections to process.

Immunohistochemistry: After sectioning, brain slices were washed once with 1x PBS to remove O.C.T. Compound. Samples were then incubated overnight at 4°C on a shaker in a 1x PBS solution containing 0.1% Triton X-100, 10% normal goat serum (NGS; Jackson ImmunoResearch, PA, USA) and primary antibodies. Sections were washed three times for 15 min each in 1x PBS. Next, brain slices were incubated at 4°C overnight on a shaker in a 1x PBS solution containing 0.1% Triton X-100, 10% NGS and secondary antibodies. Sections were washed again three times for 15 min each in 1x PBS. Finally, slices were mounted on glass microscope slides (Adhesion Superfrost Plus Glass Slides, #5075-Plus, Brain Research Laboratories, MA, USA). After the brain slices dried, DAPI-containing mounting media (Fluoromount G with DAPI, 00-4959-52, eBioscience, CA, USA) was added before protecting the slices with a coverglass (Cover glass, #4860-1, Brain Research Laboratories, MA, USA). Confocal images were acquired on a Zeiss LSM 880 confocal microscope (Zeiss, Oberkochen, Germany). For quantification of viral transduction efficiency of DRN^{SERT} and DRN^{ePet} neurons and ablation of 5-HT neurons, brain slices were imaged on a Keyence BZ-X700 microscope (Keyence, IL, USA). The following primary antibodies were used: chicken polyclonal anti-GFP (1:500; GFP-1020; Aves Labs, OR, USA), chicken polyclonal anti-mCherry (1:500; ab205402; Abcam, MA, USA), rabbit polyclonal anti-Tryptophan Hydroxylase 2 (1:500; ABN60; Millipore, MA, USA). The following secondary antibodies were used: goat anti-chicken IgY H&L Alexa Fluor 488 (1:500; ab150169; Abcam, MA, USA), goat anti-chicken IgY H&L Alexa Fluor 647 (1:500; ab150175; Abcam, MA, USA), goat anti-rabbit IgG H&L Alexa Fluor 488 (1:500; ab150077; Abcam, MA, USA), goat anti-rabbit IgG H&L Alexa Fluor 647 (1:500; ab150079; Abcam, MA, USA).

Fiber photometry (mouse): Fiber photometry was performed as previously described (Cho et al., 2017). Briefly, we used a 490 nm (211 Hz) LED for GCaMP6s excitation and a 405 nm (531 Hz) LED for isosbestic wavelength (M490F1 and M405F1, Thorlabs Inc., NJ, USA). A real-time processor (RX8-2, Tucker David Technologies, FL, USA) and custom-written software (provided by Drs. Karl Deisseroth and Tom Davidson, Stanford University) were used to control the modulation at two different frequencies. GFP and violet cleanup excitation filters (FF02-472/30-25 and FF01-400/40-25, Semrock, NY, USA) were used for excitation wavelengths. The two different excitation lights were reflected off dichroic mirrors (DMLP425 and MD498, Thorlabs) and coupled into a low auto-fluorescence 400 μm patch cord (MFP_400/430/1100-0.48_2m_FC-ZF1.25, Doric lenses) with a high NA coupler/collimator (F240FC-A, Thorlabs). The patch cord was attached to a ceramic optical fiber implanted into the mouse brain. The LED powers for both excitation wavelengths were measured with a power meter (PM100D, Thorlabs) and set to be ~70 μW at the end of the patch cord. The emitted GCaMP6s fluorescence was guided back into the patch cord to the collimator, and passed through a dichroic mirror (MD498, Thorlabs). The signal was passed through a GFP emission filter (MF525-39, Thorlabs) and then relayed to a femtowatt photoreceiver (Model 2151, Newport Co., Irvine, CA, USA) using a focusing lens (62-561, Edmunds Optics, Barrington, NJ, USA). Photoreceiver signals were fed into an RX8-2 processor through a BNC cable and were demodulated into two signals, corresponding to each LED excitation wavelength based on its modulation frequency. These signals were then digitized at a sampling rate of 382 Hz and low-pass filtered at 15 Hz. To synchronize fiber

photometry and EEG/EMG recordings, a BNC cable carrying TTL pulses from a TTL pulse generator (OTPG_8, Doric lenses, Quebec, QC, Canada) was connected to a digital input channel.

Polysomnographic recordings (mouse): During polysomnographic recordings animals were singly housed in clear Plexiglas cylindrical tubes (diameter = 15”, height = 20”) with ad libitum food and water. Mice were connected to a customized pre-amplifier (10x gain, 0.5 Hz high-pass filter, 10 Hz high-pass filter for EMG; Pinnacle Technology Inc., Lawrence, KS, USA) which was attached to a commutator (8204, Pinnacle Technology Inc.) enabling free movement. Before experiments began, mice were habituated to the recording conditions for at least 2 days. EEG/EMG signals were digitized using the OmniPlex System (Plexon, TX, USA) with a sampling rate of 1 kHz. Once data was acquired, Plexon’s proprietary file format (pl2) was converted to European data format (.edf) with MATLAB (MathWorks, MA, USA) using the EEGLAB plug-in (Schwartz Center for Computational Neuroscience, La Jolla, CA, USA).

Sleep deprivation (mouse): During the first 6 h of the light phase animals were sleep deprived by gentle handling (Eban-Rothschild et al., 2016) while monitoring their EEG and EMG signals on a computer screen. A paint brush was used to softly touch the animal whenever it exhibited reduced EMG tone and/or its EEG signal amplitudes increased. Following sleep deprivation, EEG and EMG signals were recorded for the remaining 6 h of the light phase.

Optogenetic stimulation (mouse): Patch cords connected 447 nm lasers (MDL-III-447/200mW, Opto Engine LLC, Midvale, UT, USA) via swivel commutators (fiber-optic rotary joints, FRJ_1×1_FC-FC, Doric lenses) to the optical fibers implanted in animals. Laser pulses were controlled by a TTL pulse generator (OTPG_8, Doric lenses, Quebec, QC, Canada). TTL pulses were sent simultaneously to the lasers and the Plexon acquisition system through an analog input to record stimulation time with regard to EEG/EMG recording time. Pulse width was 10 ms and an optical power meter (PM100D, Thorlabs) was used to set the laser output to 5 mW at the tip of the optical fiber. Burst optical stimulation consisted of a 3 s train of pulses at 25 Hz delivered every 10 s for 5 min. This stimulation pattern was referred to as a single trial and was repeated every 30-40 min during the light phase. Tonic optical stimulation consisted of 12.5 min of pulses at a frequency of 3 Hz, which amounts to the same number of optical stimuli per trial as for the burst stimulation condition. Trials using tonic stimulation were repeated every 30-40 min during the dark phase. In order to collect enough single trials per animal and condition, experiments were repeated three times such that every other day an animal was subject to optical stimulation. For optogenetic experiments in conjunction with fluoxetine injection, 10-20 mg/kg fluoxetine (BML-NS140-0050, Enzo Life Sciences, Inc., NY, USA) was delivered by i.p. injection 30-60 min before the start of the experiment (i.e. 30-60 min before lights on or off).

Sleep/wake analysis (mouse): SleepSign analysis software (SleepSign for Animal, Kissei Comtec Co., Nagano, Japan) was used for sleep-wake classification. Wake state was

characterized by desynchronized EEG and high EMG activity. NREM sleep was identified by synchronized EEG with high power at < 4 Hz and low EMG activity. REM sleep was defined by desynchronized EEG with high power at theta frequencies (6-9 Hz) and very low EMG tone. Sleep-wake states were assigned to 5 s non-overlapping windows of EEG/EMG signals. EEG/EMG signals from experiments were automatically scored according to arbitrarily defined threshold for delta power, theta ratio and EMG integral. Classification was then manually corrected by an experimenter (M.A.) who was blind to expressed transgene and experimental conditions.

Fiber photometry data processing and analysis (mouse): Pre-processing of fiber photometry data was performed as previously described (Cho et al., 2017; Lerner et al., 2015). First, a 4^{th} order Butterworth filter with zero-phase distortion was applied to low-pass filter at 2 Hz fiber photometry signals from the two excitation wavelengths, 490 nm and 405 nm. Using a least-squares linear fit, the 405 nm signal was aligned to the 490 nm signal. ΔF/F was then calculated according to: (490 nm signal – fitted 405 nm signal)/(fitted 405 nm signal). To analyze temporal dynamics of DRN^{SERT} activity during sleep-wake states, photometry signals from each state including 20% of the traces before and after state transitions were extracted and down-sampled to a defined sample number in order to normalize timescale (Figure 5D). After down-sampling, each episode has a total duration of 1 (a.u.). For further analysis of significant dynamics within one state episode, ΔF/F values between 10 – 20 percentile time range of an episode were compared to values between 80 – 90 percentile time range. In Figure S6E these time ranges are referred to as early and late, respectively. Only sleep-wake states which lasted for >= 30 s were considered for this analysis.

EEG spectrogram and power spectral density (mouse): EEG spectrogram plots were generated as previously described (Cho et al., 2017). Briefly, time-frequency decomposition of EEG signals was accomplished using Morlet wavelet and convolved with a complex Morlet wavelet having a Gaussian shape both in time and frequency domain around its central frequency. To estimate the power spectral density of EEG signals, the Welch method was applied. Window size was defined to be 5 s with 50% overlap between windows. Power was estimated at frequencies from 0.5 Hz to 100 Hz at 1 Hz step sizes. For optogenetic experiments, changes in power spectral density during the first minute of burst stimulation or last five minutes of tonic stimulation are shown as percentages of power estimates of one minute or five minutes before optical stimulation onset, respectively. For sleep deprivation experiments, only EEG signals from NREM bouts (>= 30 s) were considered for spectral analysis. In Figures S7J and S7K, BL refers to the average delta power in EEG signals from all NREM episodes across 12 h of undisturbed light phase. These EEG/EMG recordings were obtained during the previous light phase and were part of the 24 h EEG/EMG recordings whose analysis is shown in Figure 6C-6E. Likewise, in Figure 6F delta power in EEG signals from NREM episodes after sleep deprivation were compared to delta power in EEG signals from NREM episodes during the previous light phase EEG/EMG recordings without sleep deprivation. However, as opposed to Figures S7J and S7K, Figure 6F used NREM episodes from the corresponding time window as a comparison. Thus, average delta power from NREM episodes occurring within 0-2 h after SD were compared to average

delta power from NREM episodes occurring within 6-8 h after light phase onset in the previous light phase recording. One control animal was excluded from spectral analysis due to a large number of artifacts in EEG traces.

Quantification of efficiency and specificity of viral transgene expression (mouse): To quantify efficiency and specificity of viral transduction, optical sections were obtained via structured illumination on a Keyence BZ-X700 microscope (Keyence, IL, USA). Manual quantification was performed using the Cell Counter plugin, present in the Fiji distribution (Schindelin et al., 2012) of ImageJ (National Institutes of Health, Bethesda, MD). For samples from optogenetic and fiber photometry experiments, fluorescence micrographs were cropped to a 700 μm circle centered on the DRN. Seven to eight adjacent coronal sections, in which the tip of the optical fiber was clearly demarcated, were quantified, containing 1238 ± 98 TPH2+ cells. Efficiency was calculated as the total number of double-positive cells (i.e. transgene and TPH2 immunoreactive cells) divided by the total number of TPH2 immunoreactive cells. Specificity was calculated as the total number of double-positive cells divided by the total number of transgene-immunoreactive cells. To quantify the degree of virus-mediated ablation, epifluorescence micrographs were used. The number of TPH2 immunoreactive cells was counted in serial coronal sections, starting at the most posterior aspect of the hypothalamus and ending 15 sections posterior to the first appearance of the central lobule of the cerebellar vermis. Animals in our control cohort had >7000 and >360 5-HT neurons in the B5-B9 groups and B1-B3 groups (up to appearance of the central lobule of the cerebellar vermis), respectively. Experimental animals were excluded from analysis if they had >520 and/or <360 5-HT neurons in the B5-B9 groups and B1-B3 groups, respectively.

QUANTIFICATION AND STATISTICAL ANALYSIS

Zebrafish—For all behavioral experiments the unit of analysis for statistics is a single animal during the day or night; for optogenetic experiments the unit of analysis for statistics is a single trial (Figure 4: 6 trials per animal; Figure S5: 3 trials per animal). Number of animals whose data are shown in a panel are indicated by “n=”. Normality tests (D'Agostino & Pearson omnibus normality test; Shapiro-Wilk normality test) demonstrated that most behavioral parameters were not normally distributed. We therefore used non-parametric tests for most statistical analyses (Mann-Whitney test for two unpaired groups; Kruskal-Wallis test with Dunn’s correction for multiple comparisons for more than two unpaired groups). The data represented in Figure 2C were normally distributed, hence we used unpaired t test. Line graphs represent mean ± s.e.m. Tukey box plots were used for data presentation, and are constructed as follows: the main rectangle (box) extends from the 25^{th} to the 75^{th} percentile with the median marked by a horizontal line through the box. The inter-quantile range (IQR) is the distance between these two quartiles. The lower whisker extends to the smallest datum that is larger than 25^{th} percentile - 1.5*IQR. The upper whisker extends to the largest datum that is smaller than 75^{th} percentile + 1.5*IQR. Data points outside the Tukey range were not represented in the graphs to facilitate data presentation but were included in statistical analyses. All statistical analyses were performed using Prism 6 (GraphPad Software, San Diego, CA, USA). Data are considered to be statistically significant if $p<0.05$.

Mouse—All data shown in the figures, except for the representative examples, are represented as mean ± s.e.m. The unit of analysis for statistics is a single animal. The single trials from one animal are averaged and the average value from each animal is then used to calculate mean ± s.e.m. and to test for statistical significance. Number of animals whose data are shown in a panel are indicated by "n=". Probability in Figures 7 and S7 is calculated by taking the ratio of number of times the animal spent in a particular behavioral state at a given time point with regard to optical stimulation over the total number of single trials. The Kolmogorov-Smirnov test, Lilliefors test and Shapiro-Wilk normality test were used to test for normality. Paired and unpaired t tests were applied when all the data shown in a given panel is normally distributed, otherwise the non-parametric Wilcoxon rank sum test was applied. To compare more than two groups, one-way ANOVA was used with Bonferroni correction for multiple comparisons. The Statistics and Machine Learning toolbox in MATLAB (Mathworks) was used for statistical analyses. Data are considered to be statistically significant if $p<0.05$.

DATA AND SOFTWARE AVAILABILITY

The datasets generated and analyzed in this study are available from the corresponding author upon request.

Supplementary Material

Refer to Web version on PubMed Central for supplementary material.

Acknowledgements

We thank the Gradinaru and Prober labs for helpful discussions; Viveca Sapin, Uyen Pham, Hannah Hurley and Tasha Cammidge for zebrafish husbandry assistance, Chanpreet Singh for generating the *Tg(aanat2:ChR2-YFP)* line, Elisha D. Mackey for supervising mouse breeding, Andres Collazo for advice on 2- photon laser ablation, Justin S. Bois for advice on statistics and Catherine M. Oikonomou for critical reading of the manuscript. This work was supported by grants from the NIH (G.O. F32NS082010; V.G. RF1MH117069; D.A.P. R01NS070911, R01NS101158, R01NS095824, R01NS101665), Center for Molecular and Cellular Neuroscience of the Chen Institute (V.G.) and the Beckman Institute for CLARITY, Optogenetics and Vector Engineering Research (V.G.). G.M.C. is supported by a PGS-D from the National Science and Engineering Research Council (NSERC) of Canada. V.G. is a Heritage Principal Investigator supported by the Heritage Medical Research Institute.

REFERENCES

Adrien J (2008). Sleep and waking in mutant mice that do not express various proteins involved in serotonergic neurotransmission such as the serotonergic transporter, monoamine oxidase A, and 5-HT1A, 5-HT1B, 5-HT2A, 5-HT2C and 5-HT7 receptors In Serotonin and Sleep: Molecular, Functional and Clinical Aspects, Monti JM, Pandi-Perumal SR, Jacobs BL, and Nutt DJ, eds. (Basel: Birkhäuser), pp. 457–475.

Airhart MJ, Lee DH, Wilson TD, Miller BE, Miller MN, Skalko RG, and Monaco PJ (2012). Adverse effects of serotonin depletion in developing zebrafish. Neurotoxicol. Teratol 34 152–160. [PubMed: 21893190]

Alenina N, Kikic D, Todiras M, Mosienko V, Qadri F, Plehm R, Boyé P, Vilianovitch L, Sohr R, Tenner K, et al. (2009). Growth retardation and altered autonomic control in mice lacking brain serotonin. Proc. Natl. Acad. Sci. U. S. A 106, 10332–10337. [PubMed: 19520831]

Allers KA, and Sharp T (2003). Neurochemical and anatomical identification of fast- and slow-firing neurones in the rat dorsal raphe nucleus using juxtacellular labelling methods in vivo. Neuroscience 122, 193–204. [PubMed: 14596860]

Aston-Jones G, and Cohen JD (2005). An integrative theory of locus coeruleus-norepinephrine function: adaptive gain and optimal performance. Annu. Rev. Neurosci 28, 403–450. [PubMed: 16022602]

Azmitia EC, and Segal M (1978). An autoradiographic analysis of the differential ascending projections of the dorsal and median raphe nuclei in the rat. J. Comp. Neurol 179, 641–667. [PubMed: 565370]

Bellipanni G, Rink E, and Bally-Cuif L (2002). Cloning of two tryptophan hydroxylase genes expressed in the diencephalon of the developing zebrafish brain. Mech. Dev 119, S215–S220. [PubMed: 14516688]

Borbély AA (1982). A two process model of sleep regulation. Hum. Neurobiol 1, 195–204. [PubMed: 7185792]

Borbély AA, and Neuhaus HU (1979). Sleep-deprivation: Effects on sleep and EEG in the rat. J. Comp. Physiol 133, 71–87.

Bouhuys AL, and Van Den Hoofdakker RH (1977). Effects of midbrain raphe destruction on sleep and locomotor activity in rats. Physiol. Behav 19, 535–541. [PubMed: 206920]

Buchanan GF, and Richerson GB (2010). Central serotonin neurons are required for arousal to CO2. Proc. Natl. Acad. Sci 107, 16354–16359. [PubMed: 20805497]

Burgess HA, and Granato M (2007). Sensorimotor gating in larval zebrafish. J. Neurosci. Off. J. Soc. Neurosci 27, 4984–4994.

Cespuglio R, Walker E, Gomez M-E, and Musolino R (1976). Cooling of the nucleus raphe dorsalis induces sleep in the cat. Neurosci. Lett 3, 221–227. [PubMed: 19604890]

Chen S, Oikonomou G, Chiu CN, Niles BJ, Liu J, Lee DA, Antoshechkin I, and Prober DA (2013). A large-scale in vivo analysis reveals that TALENs are significantly more mutagenic than ZFNs generated using context-dependent assembly. Nucleic Acids Res. 41, 2769–2778. [PubMed: 23303782]

Cho JR, Treweek JB, Robinson JE, Xiao C, Bremner LR, Greenbaum A, and Gradinaru V (2017). Dorsal Raphe Dopamine Neurons Modulate Arousal and Promote Wakefulness by Salient Stimuli. Neuron 94, 1205–1219 e8. [PubMed: 28602690]

Cohen JY, Amoroso MW, and Uchida N (2015). Serotonergic neurons signal reward and punishment on multiple timescales. ELife 4, e06346.

Curado S, Stainier DYR, and Anderson RM (2008). Nitroreductase-mediated cell/tissue ablation in zebrafish: a spatially and temporally controlled ablation method with applications in developmental and regeneration studies. Nat. Protoc 3, 948–954. [PubMed: 18536643]

Dahlstroem A, and Fuxe K (1964). Evidence for the existence of monoamine-containing neurons in the central nervous system. I. Demonstration of monoamines in the cell bodies of brain stem neurons. Acta Physiol. Scand Suppl. SUPPL 232:1–55.

Dreosti E, Lopes G, Kampff AR, and Wilson SW (2015). Development of social behavior in young zebrafish. Front. Neural Circuits 9, 39. [PubMed: 26347614]

Dugovic C, and Wauquier A (1987). 5-HT2 receptors could be primarily involved in the regulation of slow-wabe sleep in the rat. Eur. J. Pharmacol 137, 145–146. [PubMed: 2956115]

Eban-Rothschild A, Rothschild G, Giardino WJ, Jones JR, and de Lecea L (2016). VTA dopaminergic neurons regulate ethologically relevant sleep-wake behaviors. Nat Neurosci 19, 1356–1366. [PubMed: 27595385]

Fisher SP, Foster RG, and Peirson SN (2013). The circadian control of sleep. Handb. Exp. Pharmacol 157–183. [PubMed: 23604479]

Frank MG, Stryker MP, and Tecott LH (2002). Sleep and sleep homeostasis in mice lacking the 5-HT2c receptor. Neuropsychopharmacology 27, 869–873. [PubMed: 12431861]

Gandhi AV, Mosser EA, Oikonomou G, and Prober DA (2015). Melatonin is required for the circadian regulation of sleep. Neuron 85, 1193–1199. [PubMed: 25754820]

Gent TC, Bandarabadi M, Herrera CG, and Adamantidis AR (2018). Thalamic dual control of sleep and wakefulness. Nat. Neurosci 21, 974–984. [PubMed: 29892048]

Goto Y, Otani S, and Grace AA (2007). The Yin and Yang of dopamine release: a new perspective. Neuropharmacology 53, 583–587. [PubMed: 17709119]

Idzikowski C, Mills FJ, and Glennard R (1986). 5-Hydroxytryptamine-2 antagonist increases human slow wave sleep. Brain Res. 378, 164–168. [PubMed: 3091188]

Iwasaki K, Komiya H, Kakizaki M, Miyoshi C, Abe M, Sakimura K, Funato H, and Yanagisawa M (2018). Ablation of central serotonergic neurons decreased REM sleep and attenuated arousal response. Front. Neurosci 12.

Jacobs BL, and Azmitia EC (1992). Structure and function of the brain serotonin system. Physiol. Rev 72, 165–229. [PubMed: 1731370]

Jacobs BL, and Fornal CA (2010). Activity of brain serotonergic neurons in relation to physiology and behavior In Handbook of the Behavioral Neurobiology of Serotonin, (Amsterdam: Elsevier/ Academic Press), pp. 153–162.

Jouvet M (1968). Insomnia and decrease of cerebral 5-hydroxytryptamine after destruction of the raphe system in the cat. Adv. Pharmacol 6, 265–279. [PubMed: 5301639]

Jouvet M (1972). The role of monoamines and acetylcholine-containing neurons in the regulation of the sleep-waking cycle. Ergeb. Physiol 64, 166–307. [PubMed: 4403272]

Jouvet M (1999). Sleep and serotonin: an unfinished story. Neuropsychopharmacology 21, 24S–27S. [PubMed: 10432485]

Kawashima T, Zwart MF, Yang C-T, Mensh BD, and Ahrens MB (2016). The Serotonergic system tracks the outcomes of actions to mediate short-term motor learning. Cell 167, 933–946.e20. [PubMed: 27881303]

Kirby LG, Pernar L, Valentino RJ, and Beck SG (2003). Distinguishing characteristics of serotonin and non-serotonin-containing cells in the dorsal raphe nucleus: electrophysiological and immunohistochemical studies. Neuroscience 116, 669–683. [PubMed: 12573710]

Koella WP, Feldstein A, and Czicman JS (1968). The effect of para-chlorophenylalanine on the sleep of cats. Electroencephalogr. Clin. Neurophysiol 25, 481–490. [PubMed: 4182602]

Lebrand C, Cases O, Adelbrecht C, Doye A, Alvarez C, El Mestikawy S, Seif I, and Gaspar P (1996). Transient uptake and storage of serotonin in developing thalamic neurons. Neuron 17, 823–835. [PubMed: 8938116]

Lerner TN, Shilyansky C, Davidson TJ, Evans KE, Beier KT, Zalocusky KA, Crow AK, Malenka RC, Luo L, Tomer R, et al. (2015). Intact-brain analyses reveal distinct information carried by SNc dopamine subcircuits. Cell 162, 635–647. [PubMed: 26232229]

Lillesaar C (2011). The serotonergic system in fish. J. Chem. Neuroanat 41, 294–308. [PubMed: 21635948]

Lillesaar C, Stigloher C, Tannhäuser B, Wullimann MF, and Bally-Cuif L (2009). Axonal projections originating from raphe serotonergic neurons in the developing and adult zebrafish, Danio rerio, using transgenics to visualize raphe-specific pet1 expression. J. Comp. Neurol 512, 158–182. [PubMed: 19003874]

Lin JY, Lin MZ, Steinbach P, and Tsien RY (2009). Characterization of Engineered Channelrhodopsin Variants with Improved Properties and Kinetics. Biophys. J 96, 1803–1814. [PubMed: 19254539]

Liu Z, Zhou J, Li Y, Hu F, Lu Y, Ma M, Feng Q, Zhang J, Wang D, Zeng J, et al. (2014). Dorsal raphe neurons signal reward through 5-HT and glutamate. Neuron 81, 1360–1374. [PubMed: 24656254]

Lovett-Barron M, Andalman AS, Allen WE, Vesuna S, Kauvar I, Burns VM, and Deisseroth K (2017). Ancestral Circuits for the Coordinated Modulation of Brain State. Cell 171, 1411–1423.e17. [PubMed: 29103613]

Marcinkiewcz CA, Mazzone CM, D'Agostino G, Halladay LR, Hardaway JA, DiBerto JF, Navarro M, Burnham N, Cristiano C, Dorrier CE, et al. (2016). Serotonin engages an anxiety and fear-promoting circuit in the extended amygdala. Nature 537, 97–101. [PubMed: 27556938]

Mathias JR, Zhang Z, Saxena MT, and Mumm JS (2014). Enhanced cell-specific ablation in zebrafish using a triple mutant of Escherichia coli nitroreductase. Zebrafish 11, 85–97. [PubMed: 24428354]

McGinty DJ, and Harper RM (1976). Dorsal raphe neurons: depression of firing during sleep in cats. Brain Res. 101, 569–575. [PubMed: 1244990]

McLean DL, and Fetcho JR (2004). Ontogeny and innervation patterns of dopaminergic, noradrenergic, and serotonergic neurons in larval zebrafish. J. Comp. Neurol 480, 38–56. [PubMed: 15515022]

Montgomery JE, Wiggin TD, Rivera-Perez LM, Lillesaar C, and Masino MA (2016). Intraspinal serotonergic neurons consist of two, temporally distinct populations in developing zebrafish. Dev. Neurobiol 76, 673–687. [PubMed: 26437856]

Monti JM (2011). Serotonin control of sleep-wake behavior. Sleep Med. Rev 15, 269–281. [PubMed: 21459634]

Monti JM, Pandi-Perumal SR, Jacobs BL, and Nutt DJ (2008). Serotonin and Sleep: Molecular, Functional and Clinical Aspects (Basel: Birkhäuser).

Mouret J, Bobillier P, and Jouvet M (1968). Insomnia following parachlorophenylalanin in the rat. Eur. J. Pharmacol 5, 17–22. [PubMed: 4305008]

Müller CP, and Jacobs BL (2010). Handbook of the behavioral neurobiology of serotonin (Amsterdam: Elsevier/Academic Press).

Murray NM, Buchanan GF, and Richerson GB (2015). Insomnia Caused by Serotonin Depletion is Due to Hypothermia. Sleep 38, 1985–1993. [PubMed: 26194567]

Narboux-Neme N, Angenard G, Mosienko V, Klempin F, Pitychoutis PM, Deneris E, Bader M, Giros B, Alenina N, and Gaspar P (2013). Postnatal growth defects in mice with constitutive depletion of central serotonin. ACS Chem Neurosci 4, 171–181. [PubMed: 23336056]

Oikonomou G, and Prober DA (2017). Attacking sleep from a new angle: contributions from zebrafish. Curr. Opin. Neurobiol 44, 80–88. [PubMed: 28391131]

Popa D, Léna C, Fabre V, Prenat C, Gingrich J, Escourrou P, Hamon M, and Adrien J (2005). Contribution of 5-HT2 receptor subtypes to sleep–wakefulness and respiratory control, and functional adaptations in knock-out mice lacking 5-HT2A receptors. J. Neurosci 25, 11231–11238. [PubMed: 16339018]

Porkka-Heiskanen T, Strecker RE, Thakkar M, Bjørkum AA, Greene RW, and McCarley RW (1997). Adenosine: a mediator of the sleep-inducing effects of prolonged wakefulness. Science 276, 1265–1268. [PubMed: 9157887]

Portas CM, and Grønli J (2008). Involvement of the 5-HT1A and the 5-HT1B receptor in the regulation of sleep and waking In Serotonin and Sleep: Molecular, Functional and Clinical Aspects, (Basel: Birkhäuser), pp. 325–369.

Portas CM, Bjorvatn B, and Ursin R (2000). Serotonin and the sleep/wake cycle: special emphasis on microdialysis studies. Prog. Neurobiol 60, 13–35. [PubMed: 10622375]

Prober DA, Rihel J, Onah AA, Sung R-J, and Schier AF (2006). Hypocretin/orexin overexpression induces an insomnia-like phenotype in zebrafish. J. Neurosci. Off. J. Soc. Neurosci 26, 13400–13410.

Qian Y, Cao Y, Deng B, Yang G, Li J, Xu R, Zhang D, Huang J, and Rao Y (2017). Sleep homeostasis regulated by 5HT2b receptor in a small subset of neurons in the dorsal fan-shaped body of Drosophila. ELife 6.

Ren J, Friedmann D, Xiong J, Liu CD, Ferguson BR, Weerakkody T, DeLoach KE, Ran C, Pun A, Sun Y, et al. (2018). Anatomically Defined and Functionally Distinct Dorsal Raphe Serotonin Sub-systems. Cell 175, 472–487.e20. [PubMed: 30146164]

Rihel J, Prober DA, Arvanites A, Lam K, Zimmerman S, Jang S, Haggarty SJ, Kokel D, Rubin LL, Peterson RT, et al. (2010). Zebrafish behavioral profiling links drugs to biological targets and rest/wake regulation. Science 327, 348–351. [PubMed: 20075256]

Saper CB, Scammell TE, and Lu J (2005). Hypothalamic regulation of sleep and circadian rhythms. Nature 437, 1257–1263. [PubMed: 16251950]

Scammell TE, Arrigoni E, and Lipton JO (2017). Neural circuitry of wakefulness and sleep. Neuron 93, 747–765. [PubMed: 28231463]

Schindelin J, Arganda-Carreras I, Frise E, Kaynig V, Longair M, Pietzsch T, Preibisch S, Rueden C, Saalfeld S, Schmid B, et al. (2012). Fiji: an open-source platform for biological-image analysis. Nat. Methods 9, 676–682. [PubMed: 22743772]

Schweimer JV, and Ungless MA (2010). Phasic responses in dorsal raphe serotonin neurons to noxious stimuli. Neuroscience 171, 1209–1215. [PubMed: 20888395]

Scott MM, Wylie CJ, Lerch JK, Murphy R, Lobur K, Herlitze S, Jiang W, Conlon RA, Strowbridge BW, and Deneris ES (2005). A genetic approach to access serotonin neurons for in vivo and in vitro studies. Proc. Natl. Acad. Sci. U. S. A 102, 16472–16477. [PubMed: 16251278]

Simonneaux V, and Ribelayga C (2003). Generation of the melatonin endocrine message in mammals: a review of the complex regulation of melatonin synthesis by norepinephrine, peptides, and other pineal transmitters. Pharmacol. Rev 55, 325–395. [PubMed: 12773631]

Singh C, Oikonomou G, and Prober DA (2015). Norepinephrine is required to promote wakefulness and for hypocretin-induced arousal in zebrafish. ELife 4.

Smith HR, Leibold NK, Rappoport DA, Ginapp CM, Purnell BS, Bode NM, Alberico SL, Kim Y-C, Audero E, Gross CT, et al. (2018). Dorsal raphe serotonin neurons mediate CO2-induced arousal from sleep. J. Neurosci 38, 1915–1925. [PubMed: 29378860]

Solarewicz JZ, Angoa-Perez M, Kuhn DM, and Mateika JH (2015). The sleep-wake cycle and motor activity, but not temperature, are disrupted over the light-dark cycle in mice genetically depleted of serotonin. Am. J. Physiol. Regul. Integr. Comp. Physiol 308, R10–7. [PubMed: 25394829]

Sommerfelt L, and Ursin R (1993). The 5-HT2 antagonist ritanserin decreases sleep in cats. Sleep 16, 15–22. [PubMed: 8456229]

Tabor KM, Bergeron SA, Horstick EJ, Jordan DC, Aho V, Porkka-Heiskanen T, Haspel G, and Burgess HA (2014). Direct activation of the Mauthner cell by electric field pulses drives ultrarapid escape responses. J. Neurophysiol 112, 834–844. [PubMed: 24848468]

Tan CL, and Knight ZA (2018). Regulation of body temperature by the nervous system. Neuron 98, 31–48. [PubMed: 29621489]

Teraoka H, Russell C, Regan J, Chandrasekhar A, Concha ML, Yokoyama R, Higashi K, Take-Uchi M, Dong W, Hiraga T, et al. (2004). Hedgehog and Fgf signaling pathways regulate the development of tphR-expressing serotonergic raphe neurons in zebrafish embryos. J. Neurobiol 60, 275–288. [PubMed: 15281067]

Torda C (1967). Effect of brain serotonin depletion on sleep in rats. Brain Res. 6, 375–377. [PubMed: 6056718]

Trueta C, and De-Miguel FF (2012). Extrasynaptic exocytosis and its mechanisms: a source of molecules mediating volume transmission in the nervous system. Front. Physiol 3.

Trulson ME, and Jacobs BL (1979). Raphe unit activity in freely moving cats: correlation with level of behavioral arousal. Brain Res 163, 135–150. [PubMed: 218676]

Ursin R (2008). Changing concepts on the role of serotonin in the regulation of sleep and waking In Serotonin and Sleep: Molecular, Functional and Clinical Aspects, (Basel: Birkhäuser), pp. 3–21.

Vanhatalo S, and Soinila S (1998). Serotonin is not synthesized, but specifically transported, in the neurons of the hypothalamic dorsomedial nucleus. Eur. J. Neurosci 10, 1930–1935. [PubMed: 9751163]

Veasey SC, Fornal CA, Metzler CW, and Jacobs BL (1995). Response of serotonergic caudal raphe neurons in relation to specific motor activities in freely moving cats. J. Neurosci 15, 5346–5359. [PubMed: 7623157]

Weitzman ED, Rapport MM, McGregor P, and Jacoby J (1968). Sleep Patterns of the Monkey and Brain Serotonin Concentration: Effect of p-Chlorophenylalanine. Science 160, 1361–1363. [PubMed: 4967983]

Westerfield M (2000). The zebrafish book A guide for the laboratory use of zebrafish (Danio rerio) (Eugene, OR: Univ. of Oregon Press).

Whitney MS, Shemery AM, Yaw AM, Donovan LJ, Glass JD, and Deneris ES (2016). Adult Brain Serotonin Deficiency Causes Hyperactivity, Circadian Disruption, and Elimination of Siestas. J. Neurosci. Off. J. Soc. Neurosci 36, 9828–9842.

Yokogawa T, Hannan MC, and Burgess HA (2012). The dorsal raphe modulates sensory responsiveness during arousal in zebrafish. J. Neurosci. Off. J. Soc. Neurosci 32, 15205–15215.

Yu H, Dickson EJ, Jung S-R, Koh D-S, and Hille B (2016). High membrane permeability for melatonin. J. Gen. Physiol 147, 63–76. [PubMed: 26712850]

Yuan Q, Joiner WJ, and Sehgal A (2006). A sleep-promoting role for the Drosophila serotonin receptor 1A. Curr. Biol. CB 16, 1051–1062. [PubMed: 16753559]

Zhdanova IV, Wang SY, Leclair OU, and Danilova NP (2001). Melatonin promotes sleep-like state in zebrafish. Brain Res. 903, 263–268. [PubMed: 11382414]

Zhuang X, Masson J, Gingrich JA, Rayport S, and Hen R (2005). Targeted gene expression in dopamine and serotonin neurons of the mouse brain. J. Neurosci. Methods 143, 27–32. [PubMed: 15763133]

Highlights

- The serotonergic system (STS) promotes sleep in zebrafish and mice
- STS disruption reduces both sleep and the homeostatic response to sleep deprivation
- Tonic stimulation of the STS induces sleep, but burst stimulation induces wake
- We propose that baseline tonic STS activity during wake generates sleep pressure

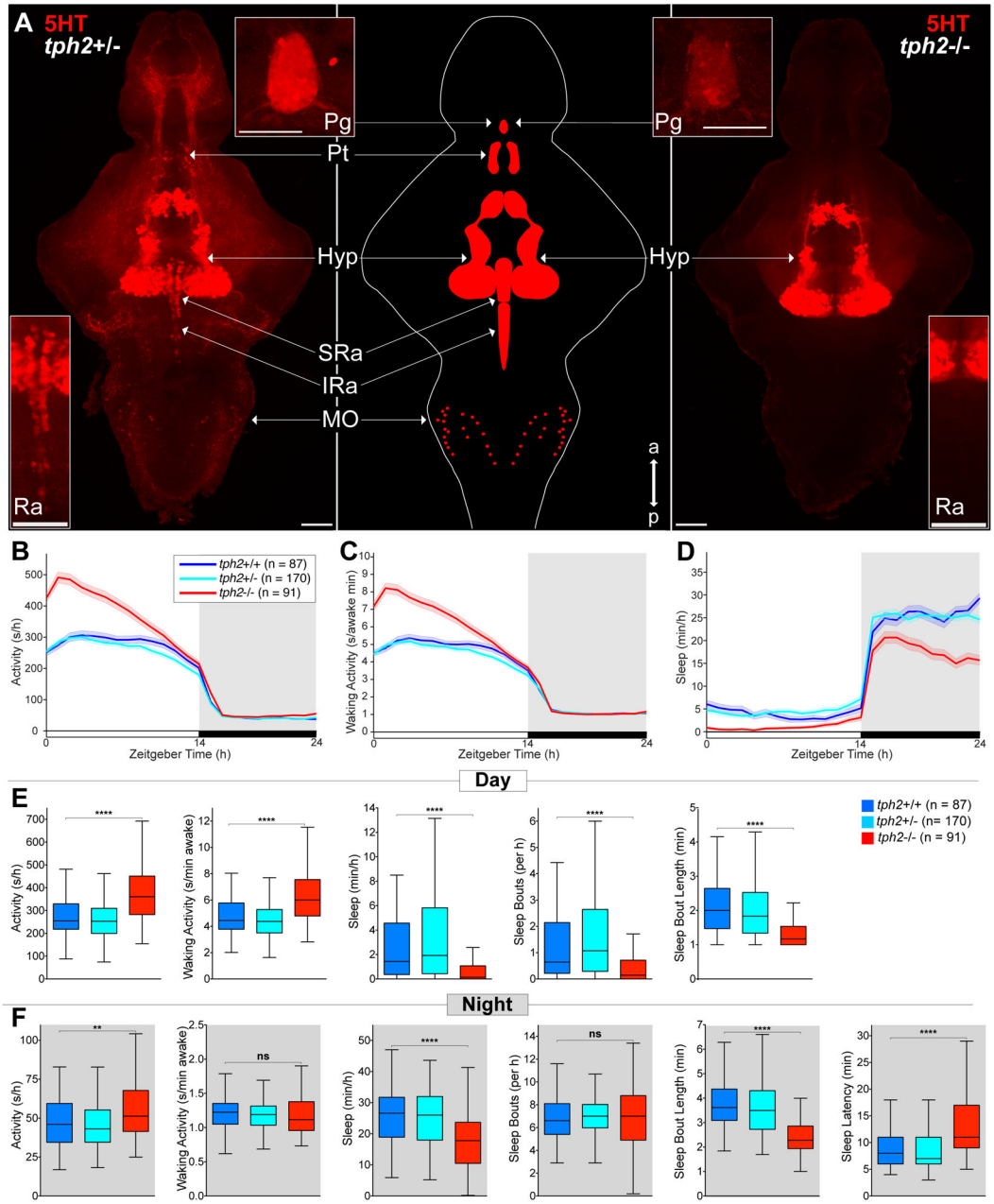

Figure 1. *tph2−/−* zebrafish are more active and sleep less.

(A) Maximum intensity projections of 5 days post-fertilization (dpf) *tph2+/−* (left) or *tph2−/−* (right) zebrafish brains immunostained for 5-HT. Middle: brain schematic. Top insets: 5-HT immunostaining of the pineal gland. Bottom insets: magnified view of the raphe. Scale bars, 50 μm; a, anterior; p, posterior; Pg, pineal gland; Pt, pretectal area; Hyp, hypothalamus; Ra, raphe; SRa, superior raphe; IRa, inferior raphe; MO, medulla oblongata.

(B-D) Activity (B), waking activity (C), and sleep (D) for *tph2+/+* (blue), *tph2+/−* (cyan), and *tph2−/−* (red) zebrafish. Line and shading represent mean ± s.e.m.

(E and F) Activity, waking activity, sleep, sleep bout number, sleep bout length during day (E) and night (F) and sleep latency at night (F).

n=number of animals. ns p>0.05, *p<0.05, **p<0.01, ***p<0.001, ****p<0.0001, Kruskal-Wallis test with Dunn's multiple comparisons test.
See also Figures S1-S3.

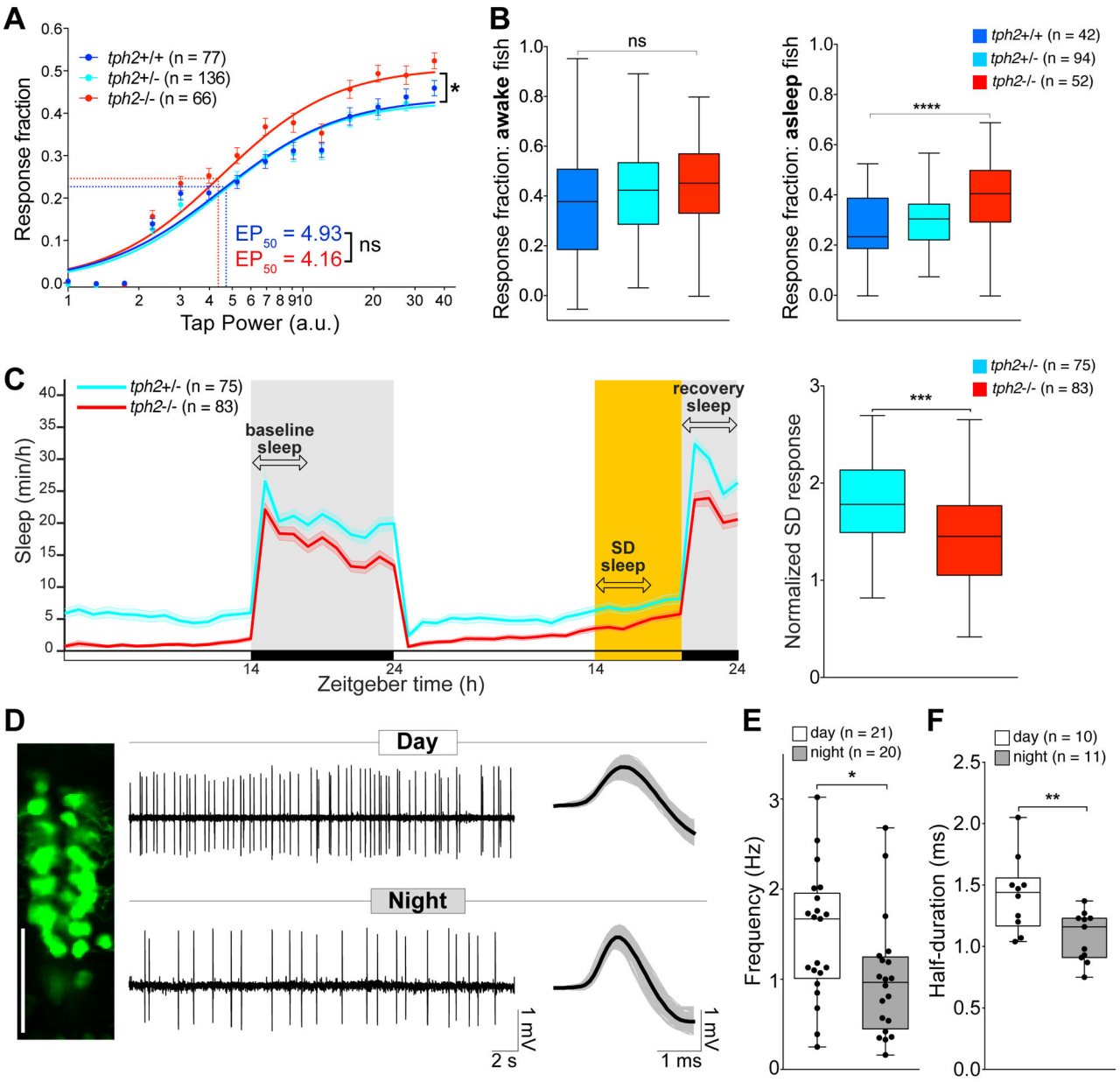

Figure 2. Zebrafish *tph2* mutants show lighter sleep and reduced rebound sleep; zebrafish raphe neurons have higher firing rates during the day.

(A) Stimulus-response curves generated using a mechano-acoustic stimulus. *tph2*−/− and sibling control animals were not significantly different in EP_{50}, but mutants exhibited increased maximal response. Data points represent mean ± s.e.m for 30 trials at each stimulus intensity (extra sum-of-squares F test).

(B) Response of awake (left) and sleeping (right) zebrafish to a mechano-acoustic stimulus. When awake, *tph2*−/− and sibling control animals responded similarly to the stimulus, but when asleep, *tph2*−/− animals were significantly more likely to respond (Kruskal-Wallis test with Dunn's multiple comparisons test).

(C) Sleep of *tph2+/−* (cyan) and *tph2−/−* (red) siblings over a 48 h period (5-6 dpf); line and shading represent mean ± s.e.m. Baseline sleep levels were established during the first 4 h (arrow in first gray box) of the first night (first grey box). Sleep deprivation during the first 6 h of the second night was achieved by maintaining daytime white light illumination (yellow shaded box). SD sleep is defined as the sleep during the first 4 h of the sleep deprivation period (arrow in yellow box). Recovery sleep is sleep during the first 4 h after lights-off (arrow in second gray box). Normalized SD response (right) is calculated as recovery sleep / (baseline sleep – SD sleep) (unpaired t test).

(D) Spontaneous firing of representative GFP-positive raphe neurons of *Tg(tph2:eGFP)* zebrafish during the day (top) and night (bottom). A single plane image of the raphe from a *Tg(tph2:eGFP)* 5 dpf zebrafish immunostained for eGFP is shown. Traces on the right show the waveform of action potentials. Black traces represent the average and gray traces represent 748 sorted events during the day and 420 sorted events at night.

(E-F) Spontaneous spike firing frequency (E) and half-duration of spontaneous action potentials (F) of GFP-positive raphe neurons of *Tg(tph2:eGFP)* animals during the day and night (Mann-Whitney test).

n=number of animals (A-C) or neurons (E, F). ns $p>0.05$, *$p<0.05$, **$p<0.01$, ***$p<0.001$, ****$p<0.0001$.

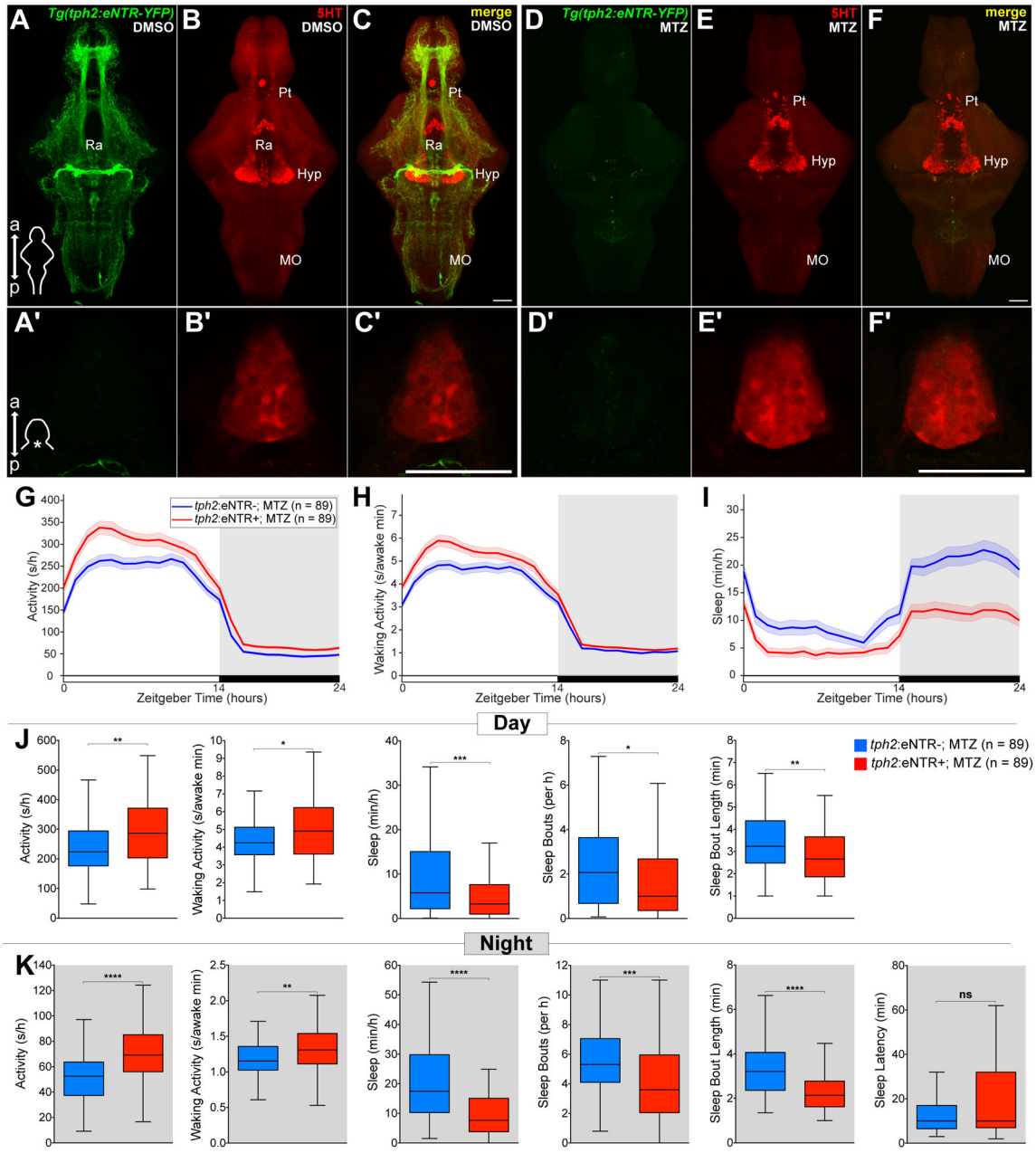

Figure 3. Chemogenetic ablation of the raphe results in decreased sleep in zebrafish.

(A-F) Maximum intensity projections of brains (A-F) and single plane images of pineal glands (A'-F') from 5 dpf *Tg(tph2:eNTR-YFP)* zebrafish treated with DMSO vehicle (A-C, A'-C') or MTZ (D-F, D'-F'), and immunostained for 5-HT and YFP. Scale bars, 50 μm; a, anterior; p, posterior; Pt, pretectal area; Hyp, hypothalamus; Ra, raphe; MO, medulla oblongata.

(G-I) Activity (G), waking activity (H), and sleep (I) for 5 dpf *Tg(tph2:eNTR-YFP)* (red) and non-transgenic sibling control (blue) zebrafish treated with MTZ. Line and shading represent mean ± s.e.m.

(J and K) Activity, waking activity, sleep, sleep bout number, sleep bout length during day (J) and night (K) and sleep latency at night (K). n=number of animals. ns $p>0.05$, *$p<0.05$, **$p<0.01$, ***$p<0.001$, ****$p<0.0001$, Mann-Whitney test.

See also Figure S4.

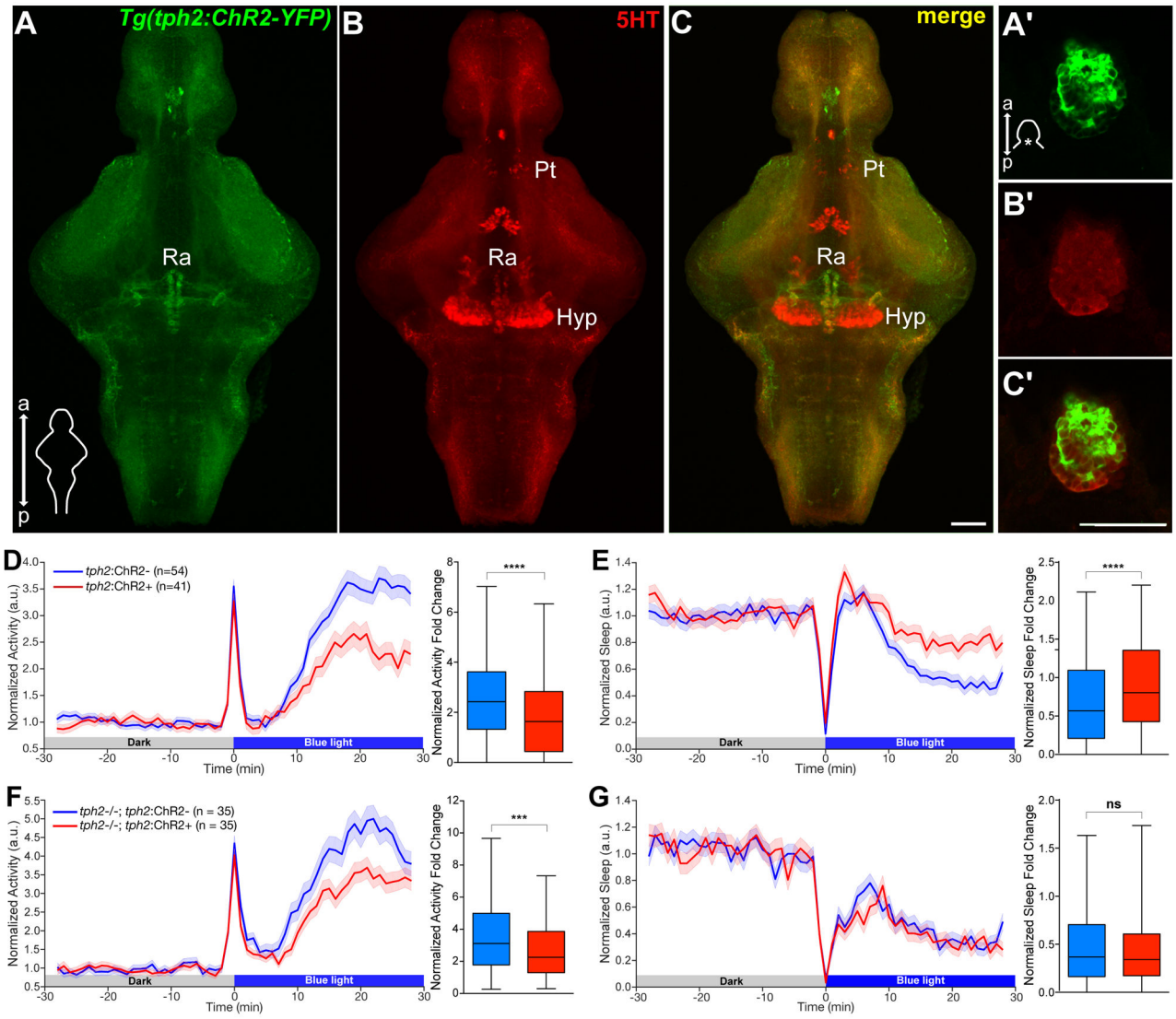

Figure 4. Optogenetic stimulation of the raphe results in reduced locomotor activity and increased sleep in zebrafish.

Maximum intensity projections of brains (A-C) and single plane images of pineal glands (A'-C') from 5 dpf *Tg(tph2:ChR2-YFP)* zebrafish immunostained for 5-HT and YFP. Scale bars, 50 μm; a, anterior; p, posterior; Pt, pretectal area; Hyp, hypothalamus; Ra, raphe.

(D and E) Left: normalized locomotor activity (D) and sleep (E) of 5 dpf *Tg(tph2:ChR2)* (red) and non-transgenic sibling control (blue) zebrafish before and during exposure to blue light. Right: normalized locomotor activity (D) and sleep (E) fold change during illumination.

(F and G) Same as (D) and (E) but in *tph2−/−* animals.

n=number of animals; 6 trials per animal. ns p>0.05, ***p<0.001, ****p<0.0001, Mann-Whitney test.

See also Figure S5.

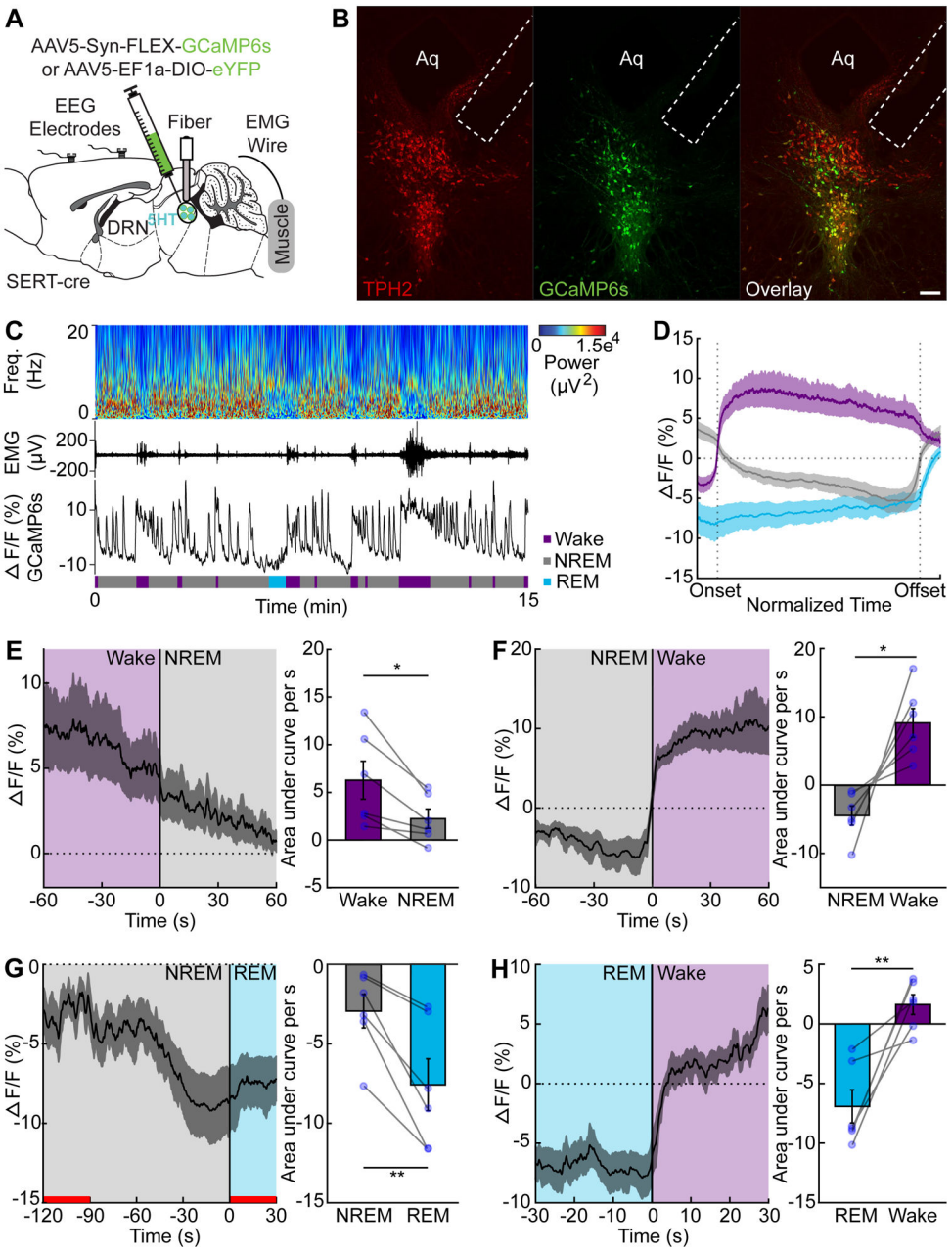

Figure 5. DRN neuronal activity correlates with sleep-wake states in mice.

(A) Experimental setup.

(B) Representative images of GCaMP6s+ neurons (green) co-localized with TPH2+ neurons (red). Scale bar, 100 μm. Aq, aqueduct.

(C) Representative DRN $^{\text{SERT-GCaMP6s}}$ mouse spectrogram, EMG and fiber photometry traces over time across different sleep-wake states.

(D) Temporal dynamics of DRN$^{\text{SERT}}$ activity during wake (purple), NREM (grey) and REM (blue) episodes within normalized time.

(E-H) DRN$^{\text{SERT}}$ activity across wake to NREM (E), NREM to wake (F), NREM to REM (G) and REM to wake (H) transitions (left) and quantification of area under the curve (right).

Statistical comparisons are based on the full time window shown (E,F,H) or on the time periods indicated by red lines (G).

Data represent mean ± sem. n = 6 mice, paired t test, *p<0.05, **p<0.01. See also Figure S6.

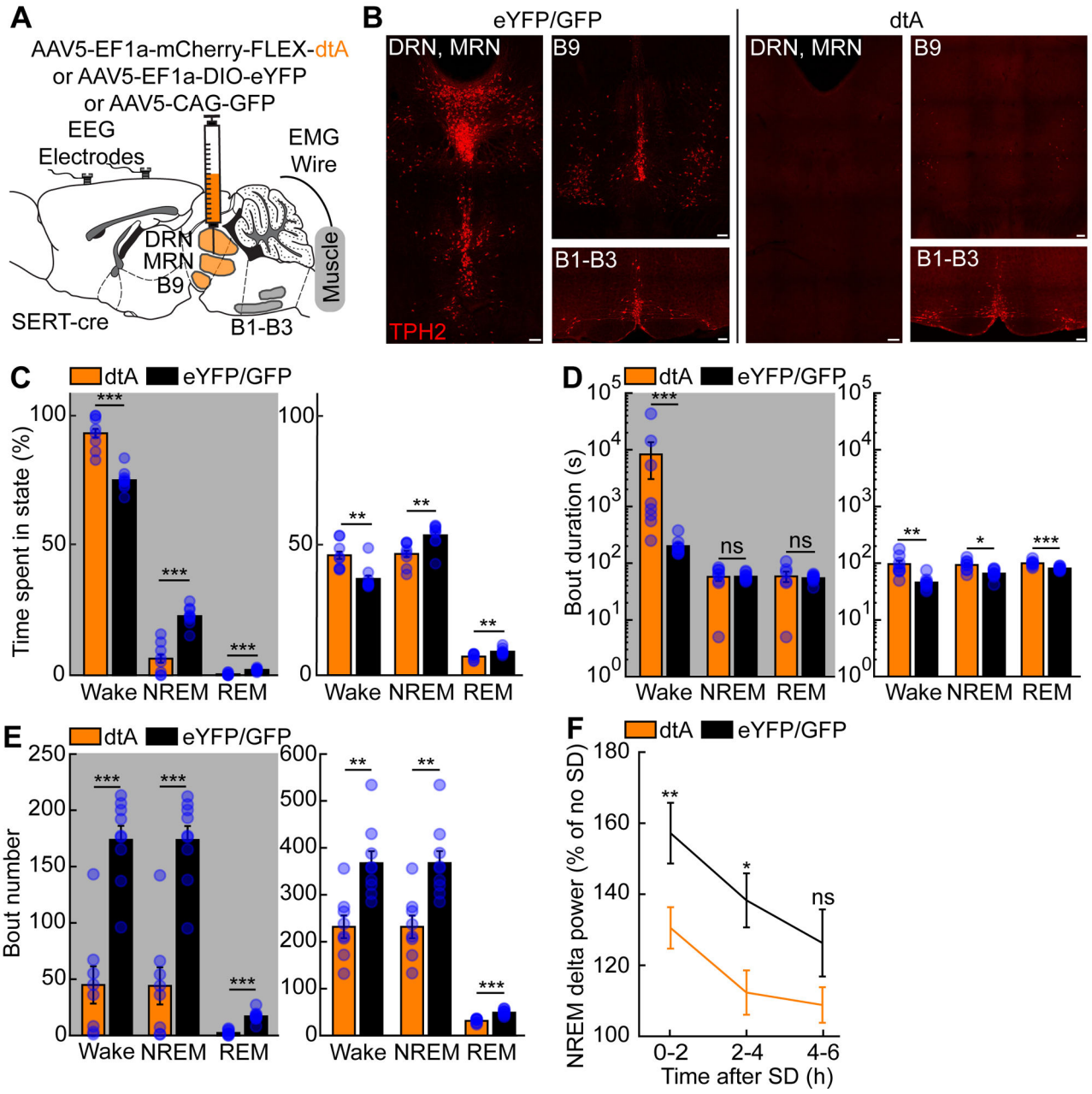

Figure 6. Ablation of murine raphe leads to increased wakefulness and impairs the homeostatic response to sleep deprivation.

(A) Experimental setup.

(B) Representative images of TPH2+ neurons (red) from SERT-cre mice injected with either AAV5-EF1a-DIO-eYFP (left) or AAV5-EF1a-mCherry-FLEX-dtA (right). Scale bar, 100 μm.

(C) Percentage of time spent in the wake, NREM and REM states during the dark (grey shading) and light phase from 24 h polysomnographic recordings.

(D-E) Duration (D) and number (E) of wake, NREM and REM bouts during the dark and light phase.

(F) Change in delta power across NREM episodes in animals subjected to 6 h of sleep deprivation (SD) at the beginning of the light phase compared to undisturbed sleep from previous light phase (no SD).
n=8 for B5-B9$^{SERT\text{-}dtA}$, n=9 for B5-B9$^{SERT\text{-}eYFP}$ or B5-B9^{GFP}, two-sided Wilcoxon rank sum test, ns $p>0.05$, *$p<0.05$, **$p<0.01$, ***$p<0.001$. See also Figure S7.

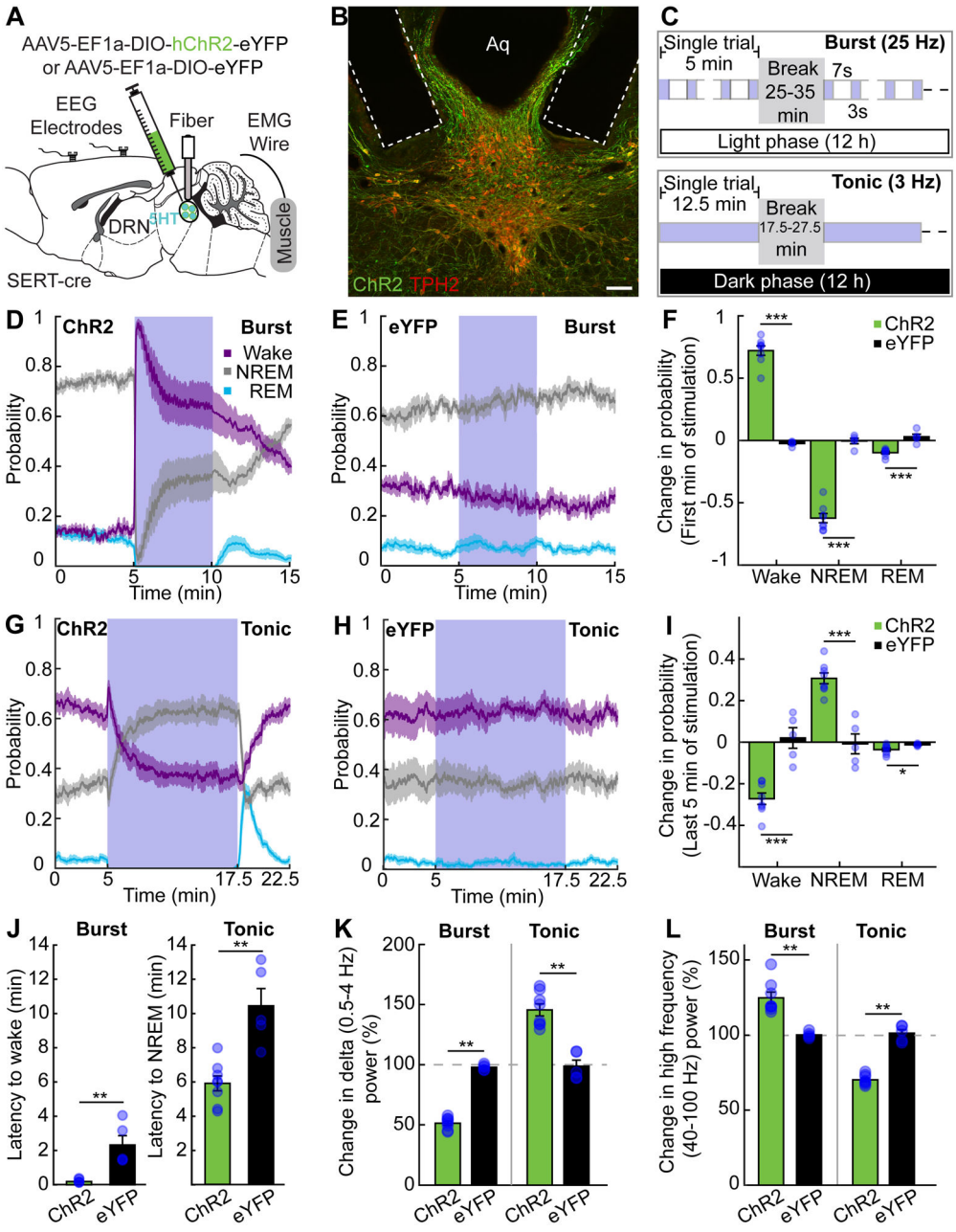

Figure 7. Optogenetic stimulation of DRN neurons has bidirectional mode-dependent effects on mouse sleep.

(A) Experimental setup.

(B) Representative images of ChR2+ neurons (green) co-localized with TPH2+ neurons (red) from a SERT-cre mouse. Scale bar, 100 μm.

(C) Burst and tonic stimulation paradigms.

(D-E) State probability trace before, during and after burst stimulation of $DRN^{SERT\text{-}ChR2}$ (D) or $DRN^{SERT\text{-}eYFP}$ (E) mice. Blue box indicates laser stimulation period.

(F) Quantification of (D) and (E) (unpaired t test).

(G-H) State probability trace before, during and after tonic stimulation of $DRN^{SERT\text{-}ChR2}$ (G) or $DRN^{SERT\text{-}EYFP}$ (H) mice.
(I) Quantification of (G) and (H) (unpaired t test).
(J) Latency to wake after burst stimulation onset in $DRN^{SERT\text{-}ChR2}$ compared to $DRN^{SERT\text{-}eYFP}$ mice (left); latency to NREM after tonic stimulation onset in $DRN^{SERT\text{-}ChR2}$ mice compared to $DRN^{SERT\text{-}eYFP}$ mice (right) (two-sided Wilcoxon rank sum test).
(K-L) Power spectral density of frontal EEG delta (K) or high frequency (L) power upon burst stimulation onset (first min of stimulation) and over the course of tonic stimulation (last five min of stimulation) (two-sided Wilcoxon rank sum test).
n=8 for $DRN^{SERT\text{-}ChR2}$; n=5 for $DRN^{SERT\text{-}eYFP}$; *p<0.05, **p<0.01, ***p<0.001. See also Figures S6 and S7.

KEY RESOURCES TABLE

REAGENT or RESOURCE	SOURCE	IDENTIFIER
Antibodies		
Rabbit polyclonal anti-5-HT	MilliporeSigma	Cat# S5545; RRID:AB_477522
Chicken polyclonal anti-GFP	Aves Labs	Cat# GFP-1020; RRID: AB_10000240
Chicken polyclonal anti-mCherry	Abcam	Cat# ab205402; RRID: AB_2722769
Mouse monoclonal anti-DsRed	Santa Cruz Biotechnology	Cat# SC-390909
Rabbit polyclonal anti-Tryptophan Hydroxylase 2	Millipore	Cat# ABN60; RRID: AB_10806898
Goat anti-Chicken IgY (H+L) Secondary Antibody, Alexa Fluor 488	Invitrogen	Cat# A-11039; RRID: AB_2534096
Goat anti-Rabbit IgG (H+L) Cross-Adsorbed Secondary Antibody, Alexa Fluor 568	Invitrogen	Cat# A-11011; RRID: AB_143157
Goat anti-chicken IgY H&L Alexa Fluor 488	Abcam	Cat# ab150169; RRID: AB_2636803
Goat anti-chicken IgY H&L Alexa Fluor 647	Abcam	Cat# ab150175; RRID: AB_2732800
Goat anti-rabbit IgG H&L Alexa Fluor 488	Abcam	Cat# ab150077; RRID: AB_2630356
Goat anti-rabbit IgG H&L Alexa Fluor 647	Abcam	Cat# ab150079; RRID: AB_2722623
Chemicals, Peptides, and Recombinant Proteins		
Quipazine maleate salt	MilliporeSigma	Cat# Q1004
Buspirone hydrochloride	MilliporeSigma	Cat# B7148
4-chloro-DL-phenylalanine methyl ester hydrochloride (pCPA)	MilliporeSigma	Cat# C3635
Metronidazole	MP Biomedicals	Cat# 0215571080
Euthasol	VWR	Cat# 102094-104
Fluoxetine HCl	Enzo Life Sciences	Cat# BML-NS140-0050
O.C.T. compound	VWR	Cat# 102094-104
16% paraformaldehyde	ThermoFisher Sci.	Cat# 15710
Normal goat serum	ThermoFisher Sci.	Cat# NC9660079
Collagenase	MilliporeSigma	Cat# C9891
Vectashield	Vector laboratories	Cat# H-1000; RRID:AB_2336789
Fluoromount G with DAPI	ThermoFisher Sci.	Cat# 00-4959-52
alpha-bungarotoxin	Tocris	Cat# 2133
tricaine	MilliporeSigma	Cat# A5040
Experimental Models: Organisms/Strains		
Zebrafish: *tph2* ct817 mutant	(Chen et al., 2013)	RRID: ZDB-ALT-131122-14
Zebrafish: *aanat2* ct801 mutant	(Gandhi et al., 2015)	RRID: ZDB-ALT-131122-2
Zebrafish: *Tg(tph2:eGFP)* ct864Tg	This paper	RRID: ZDB-ALT-190508-1
Zebrafish: *Tg(tph2:ChR2-YFP)* ct865Tg	This paper	RRID: ZDB-ALT-190508-2

REAGENT or RESOURCE	SOURCE	IDENTIFIER
Zebrafish: *Tg(tph2:eNTR-YFP)* ct866Tg	This paper	RRID: ZDB-ALT-190508-3
Mouse: SERT-cre (Zhuang et al., 2005)	Jackson Laboratory	Stock No: 014554; RRID:IMSR_JAX:014554
Mouse: ePet-cre (Scott et al., 2005)	Jackson Laboratory	Stock No: 012712; RRID:IMSR_JAX:012712
Oligonucleotides		
Primer: *tph2* promoter Forward: TGTCTTCCTGCCATTAGTCTG	This paper	N/A
Primer: *tph2* promoter Reverse: TTAATATGGCAAAGGTAGTTTTTTTTATC	This paper	N/A
Primer: *tph2* mutant genotyping primer 1: AGAACTTACAAAACTCTATCCAACTC	This paper	N/A
Primer: *tph2* mutant genotyping primer 2: AGAGAGGACAACATCTGGGG	This paper	N/A
Primer: *tph2* mutant genotyping primer 3: TAATCATGCAGTCCGTTAATACTC	This paper	N/A
Virus strains		
AAV5-Syn-FLEX-GCaMP6s	Penn Vector Core	AV-5-PV2821
AAV5-Syn-FLEX-GCaMP6s	Addgene	100845-AAV5
AAV5-Ef1a-DIO-ChR2(H134R)-eYFP	Penn Vector Core	AV-5-20298P
AAV5-Ef1a-DIO-eYFP	Penn Vector Core	AV-5-27056
AAV5-mCherry-flex-dtA	UNC Vector Core	N/A
AAV5-CAG-GFP	Addgene	37825-AAV5
Software and Algorithms		
MATLAB R2017b	Mathworks	RRID:SCR_001622
EEGLAB plug-in	Swartz Center for Comp. Neuro.	RRID:SCR_007292
SleepSign 3.0	Kissei Comtec	http://www.sleepsign.com
Prism6	GraphPad	RRID:SCR_002798
Image J	PMID:22930834	RRID:SCR_002285
Other		
96-well plate	GE Healthcare Life Sciences	Cat#:7701-1651
MicroAmp Optical Adhesive Film	Thermo Fisher Scientific	Cat#: 4311971